Modulation of magnetic properties of magnetic thin films using flexible and ferroelectric substrates

アマニ, ハルビー

KYUSHU UNIVERSITY
GRADUATE SCHOOL OF SCIENCE

A THESIS SUBMITTED FOR THE DEGREE OF

DOCTOR OF PHILOSOPHY

Modulation of magnetic properties of magnetic thin films using flexible and ferroelectric substrates

by

Amany Elsayed Harby

Supervisor: **Professor Takashi Kimura**

March, 2022

Abstract

Electric-field manipulation of magnetic properties in multiferroic heterostructures is considered an optimistic way of authorizing memory and magnetic microwave devices with ultralow power consumption. Recently, multiferroic materials that possess both ferroelectricity (FE) and ferromagnetism (FM) provide a simple and effective way to realize electric field control of magnetism through the converse magnetoelectric (CME) coupling effect, i.e electric field control of magnetism without the need for magnetic fields.

Obtaining the magnetoelectric coupling in multiferroic heterostructures mainly focuses on the strain effect. In which the electric field produces strains inside FE layer which are transferred to the FM layer by converting magnetostrictive effect, resulting in high electric field modulation of the magnetic properties of the FM layers. On the other hand, it has been reported that the charges at the FM/FE interface can also act as a medium for the electric field modulation of magnetism, either through the electrostatic accumulation of spin-polarized charges or by the interfacial orbital reconstruction.

In this Ph.D. thesis three main topics were discussed

1- The magnetic and magnetostrictive properties of FeSiB film on two different substates Fz:Si and Polyimide.

2- The magnetoelectric properties of the multiferroic heterostructure FeSiB/PMN-0.3PT with different film thicknesses.

3- The magnetoelectric properties of the NiFe/Pt/CoFeB/PMN-0.3PT multilayer multiferroic heterostructure.

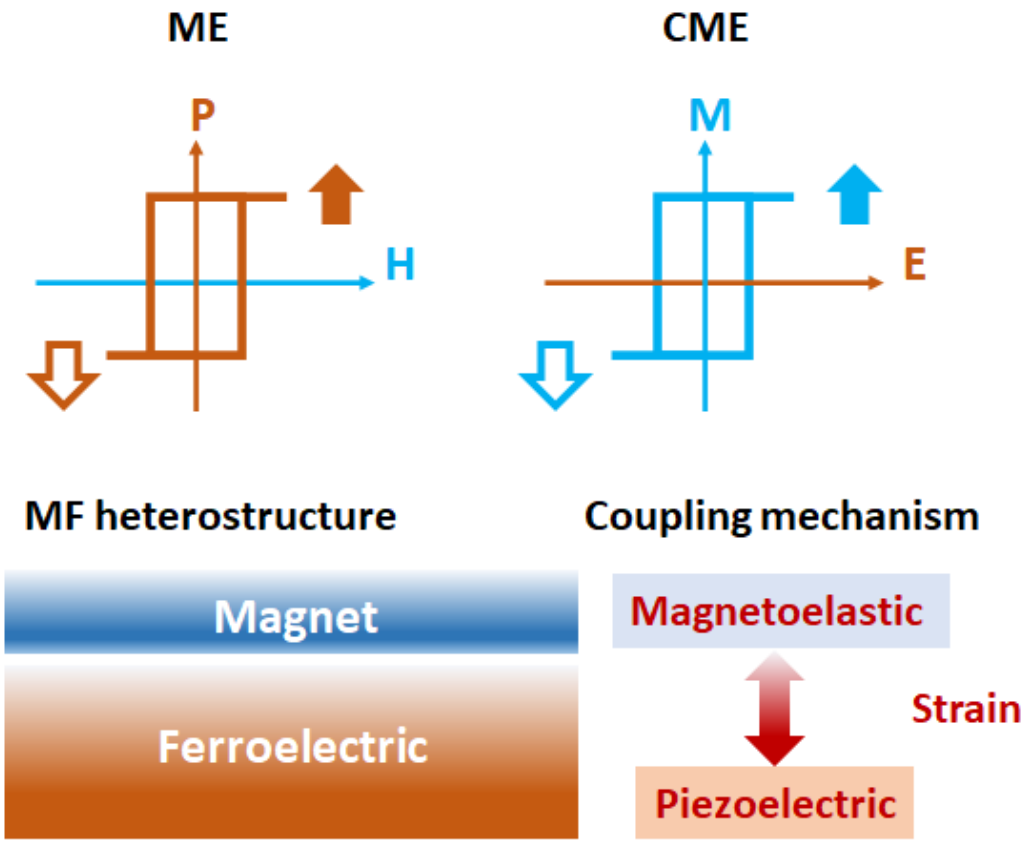

Figure 1: Illustration of magnetoelectric coupling in multiferroic heterostuctures.

In order to study the magnetoelectric properties of a FM/FE multiferroic heterostructure, we have chosen FeSiB as a FM layer. Generally, amorphous FeSiB thin films presenting magnetostriction have been investigated for decades for energy and sensors applications. They are very soft magnetic films, with high magnetization saturation. For better understanding of our chosen FM layer properties, we first studied the statics magnetostrictive properties of the amorphous FeSiB film on two different substates Fz:Si and Polyimide (with different curvatures) to confirm the magnetic and magnetostrictive properties of FeSiB. Then, we studied the magnetoelectric (ME) properties of the multiferroic heterostructure by depositing the FM magnetostictive FeSiB amorphous film with a wide range of thicknesses (10,20,50 and 100 nm) on the top of piezoelectric substrate PMN-0.3PT. After that ferroelectric, magnetic and ME properties were studied through static and dynamics measurements. We also performed the magnetoelectric measurements for the tri-layer multiferroic heterostructure NiFe/Pt/CoFeB/PMN-PT which provides an efficient way to study the effect of the electric field on the coupling/uncoupling of different combined magnetic systems.

As a result, we obtained high, non-volatile, and curvature/thickness dependent changes in the magnetic properties of our studied magnetic films. The high electrical tuning of the magnetic properties of our studied heterostructures was understood through stain and charge co-mediated mechanisms, which is the interaction between two relating coupling mechanisms consisting of the strain effect and the interfacial charge effects. From our results also we confirmed that, charge effects may become remarkable only when the thickness of the magnetic film and/or the heterostructure become small.

We believe that these interesting results indicate that the combination of the magneto-striction and high piezoelectric substrate provides the efficient modulation of the magnetic properties through the strain effect. We also can confirm that our heterostructures show a high potential for memory and energy storage applications.

Acknowledgments

I take the opportunity to acknowledge all those who directly or indirectly helped me throughout this interesting journey.

First of all, I would like to address my honest appreciation to all the members of the defense committee, Prof. Takashi Kimura, Prof. Akihiro Mitsuda, and Prof. Hiromi Yuasa for their contributions and comments.

Foremost, I would like to express my deep sense of gratitude to my supervisor Prof. Takashi Kimura from the early beginning for accepting me as a Ph.D. student in his group. Also, I would like to thank him for his kindness, patient guidance, lively discussion, and expert advice through my Ph.D. study. On the other hand, I have been extremely lucky to have a supervisor who cared so much about the safety of his students before and after the Corona pandemic. He always provided a friendly environment to work and study in our research group. I have learned a lot of useful things being one of his lab members.

Many thanks are given to all staff in Physics Department, Faculty of Science, Kyushu University especially Prof. Kohi Ohnishi and Ishima-San for supporting me a lot during my stay in Japan.

I would like to thank Dr. Shaoji Hu for supporting me a lot during my PhD study. He helped me a lot by teaching me new experimental techniques and helped me through his continuous and good scientific discussions. Also, he provided me the support and advice many times.

I would like also to thank my lab member, Dr.Md Kamaruzzaman who provides

me the continuous support. I want to thank also Ito-san, Matsuda-san, Obinata-san, Nakata-san, Imori-san and Augus, and all my colleagues for even the partial support they gave me during my Ph.D. study.

Also, I would like to thank the Ministry of Higher Education of Egypt to offer me the scholarship to conduct my PhD in Japan.

Finally, and most importantly, I would like to thank my lovely family my mother, sisters, and my brother for their unstinted moral support, encouragement, and wishes throughout the course of my stay in Japan. I want to thank especially my mother for her patience in being far away from her, especially during the Corona pandemic, and her constant concern for me and her daily support. Despite the distance, I have never felt lonely because they are always with me, encouraging me and supporting me in my times of weakness and distress.

In the end, I would like to say that I enjoyed my Ph.D journey and as well my stay in Japan Which would not have happened without the support of all those kind people.

To my family.

Contents

List of Figures

Chapter 1

Introduction

1.1 Background and motivation

Magnetization tuning undergoes colossal research interest during the last decade due to its great fundamental and technological importance with broad application prospects from magnetic memory devices, novel magnetoelectric (ME) sensors to high-frequency microwave devices [1–4]. However, tuning magnetization by the old conventional ways consumes a high amount of energy. Thus, a notably and promising way depends on an electric field to tune or control magnetization with minimal power dissipation[5–7].

Recently, multiferroic materials that possess both ferroelectricity (FE) and ferromagnetism (FM) provide a simple and effective way to realize electric field control of magnetism through the converse ME coupling effect, i.e electric field control of magnetism without the need for magnetic fields [8, 9]. However, most single-phase multiferroic (MF) materials are usually characterized by low permittivity or a low permeability at room temperature and also exhibit weak ME coupling, which limits their application[10]. Besides, these materials are often complicated to fabricate, potentially leading to electrical-leakage problems due to structural defects and impurities[11]. The studies is focusing on the use of multiferroic thin film heterostructures of ferromagnetic/ferroelectric materials as a composite material which typically exhibits

very large ME coupling (compared to that of single-phase multiferroics) above room temperature[12]. ME effects are realized via cross-coupling between piezoelectric and magnetostrictive properties of the FE and FM layers, respectively[13, 14]. A common and easy fabrication method to obtain multiferroics is to deposit ferromagnetic films on a ferroelectric/relaxor- ferroelectric single-crystal substrate such as PMN-PT, which displays a high anisotropic in-plane piezoelectric coefficient[15]. This anisotropic in-plane piezoelectric coefficient provides an outstanding opportunity for achieving a large change of in-plane uniaxial anisotropy, and consequently large ferromagnetic properties tunability via inverse magnetoelastic coupling[16]. Obtaining the magnetoelectric coupling in multiferroic heterostructures mainly focus on three leading mechanisms including strain mediated [17, 18], charge carriers [19], and exchange bias[20]. The most investigated and well-known mechanism is the strain mediated, in which the electric field produces strains inside FE layer which are transferred to the FM layer by convert magnetostrictive effect, resulting in high electric field tunability of the magnetic properties of the examined structures. On the other hand, in the charge mediated mechanism, electric field induces charge mediated coupling across FM/FE interfaces also adjusts the charge carrier concentrations at the FM layers via an accumulation or depletion process depending on the direction of FE polarization[21]. it seems that the coexistence of more than one mechanism that can contribute to controlling the magnetism in multiferroic heterostructure is a good way that could lead to significantly enhanced ME coupling in multiferroic heterostructures.

In addition, ferromagnetic thin films with amorphous structures tend to have an absence of atomic long-range order (only a random short-range order exists), which leads to a net zero magnetocrystalline anisotropy coefficient [22] compared to crystalline thin films. Moreover, Fe-based amorphous alloys display preferred magnetic properties compared with conventional soft-magnetic crystalline materials, which contain high saturation magnetic flux density (B_s), low coercivity (H_c), high permeability (μe)[23]. These alloys have gradually taken important roles in energy conservation

and eco-friendly applications and have been widely used in various electric devices. Furthermore, alloys based on the FeSiB system have drawn interest because of their magnetostrictive and soft magnetic properties displayed in the amorphous form which leads to high E-field magnetization tunability in multiferroic structures[24]. Thus, the magnetic properties such as the direction of the anisotropy in the FeSiB thin-film can be controlled according to the direction of inner stress by inverse-magnetostriction [25]. In amorphous alloys, anisotropy arises originally from magnetoelastic effects caused by internal stresses produced during the fabrication process[26]. These internal stresses are distributed in such a way that the volume average of each component of the stress tensor disappears, but locally these stresses are not zero. Therefore, the domains are oriented parallel or perpendicular to the local stress axis depending on the spontaneous magnetostriction of the material.

1.2 Outlines of the chapters

In this thesis we studied the strain effect and the electric field modulation of magnetic properties of ferromagnetic thin films in multiferroic heterostructures through the convert magnetoelectric coupling effect. The experimental results are introduced from chapter 4 to 6 as shown in fig.1.1. A brief summary of each chapter is shown as follows.

Chapter 1 : gives an introduction and the motivation of this thesis.

Chapter 2 : describes the theoretical background related to this thesis.

Chapter 3 : provides the information about the heterostructure fabrication and experimental methods that were used.

Chapter 4 : shows the effect of the curved polyimide substrate on the uniaxial magnetic anisotropy of FeSiB thin film. As a result a strong modulation of the uniaxial magnetic anisotropy is obtained by depositing FeSiB film on top of pre-bent polyimide sheets with positve and negative curvatures. This modulation can be under-

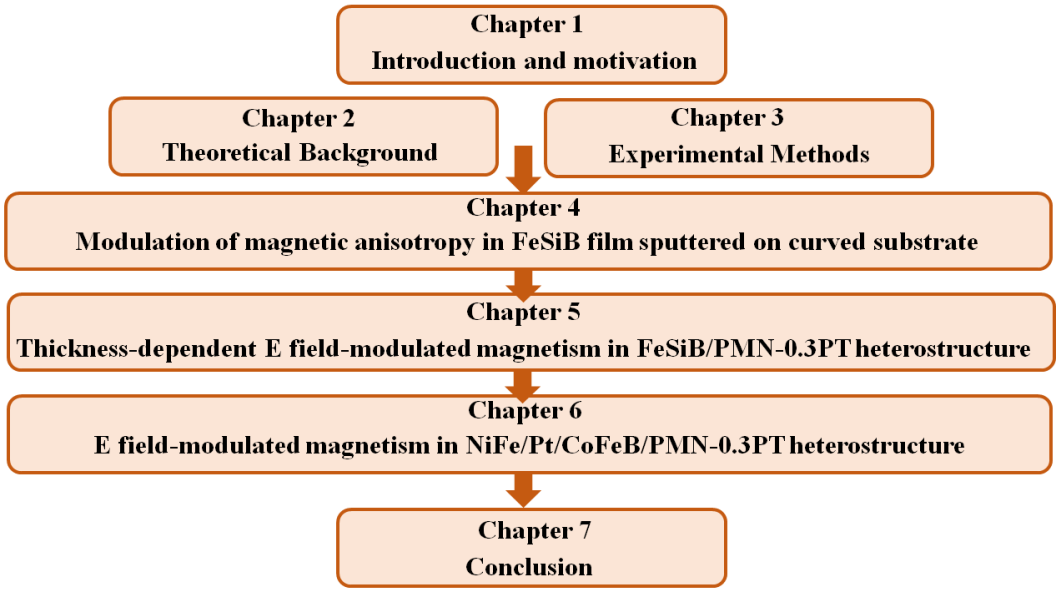

Figure 1.1: Flow chart of the chapters in this thesis.

stood through the magnetoelastic property of FeSiB film.

Chapter 5 : represents the thickness dependent of E field modulation of the magnetoelectric coupling of FeSiB/PMN-PT multiferroic heterostructure. As a result we found a strong and non-volatile E field modulation of the static and dynamic magnetic properties of FeSiB film through the cooperation of the charge and strain effect. Also, this structure showed a very high convert magnetoelectric constant near to $1x10^{-4}$ s/m.

Chapter 6 : shows the E field modulation of the magnetic properties and coupling/uncoupling behavior of the magnetic tri-layer NiFe/Pt/CoFeB/PMN-PT multiferroic heterostucture. As a result the E field shows a large and non-volatile effect of the static and dynamic magnetic properties and on the coupling behavior of the tri-layer system. The E field modulation of the magnetic properties can be understood by introducing stains at the interface layer through the combined piezoelectric and magnetoelastic properties of the MF heterostructure. The structure also showed a high convert magnetoelectric coupling of $7x10^{-5}$ s/m.

Chapter 7 : gives the conclusion of the thesis.

Chapter 2

Theoretical background

2.1 Magnetism and Magnetic Materials

The origin of magnetism is first understood in a free atom that has a magnetic dipole moment [27] even with the absence of an external magnetic field. This can be attributed to the electronic structure existing in the free atom [28], as shown Fig. 2.1. First, unpaired electrons circulating the nucleus in the atomic orbitals have orbital angular momenta, which create the atomic magnetic moment. This is just like the circulating currents made from charged particles producing a magnetic field. Second, each individual electron has an angular momentum, which also creates the "spin" magnetic moment. Moreover, both of magnetic moments, as a result of electrons orbital motion and spin themselves respectively, can be coupled, which is called spin-orbit coupling [28]. The coupling also includes orbit-orbit coupling and spin-spin coupling among electrons, which give a total atomic magnetic moment. After understanding the atomic origin of the magnetism, the next focus is on the magnetic materials, although only brief introduction is made except for ferromagnetic materials.

Magnetic materials can be categorized into the following classes: diamagnetic, paramagnetic, ferromagnetic (FM) and antiferromagnetic (AFM). Materials are classified as diamagnetic when spontaneous opposing field is induced under an external mag-

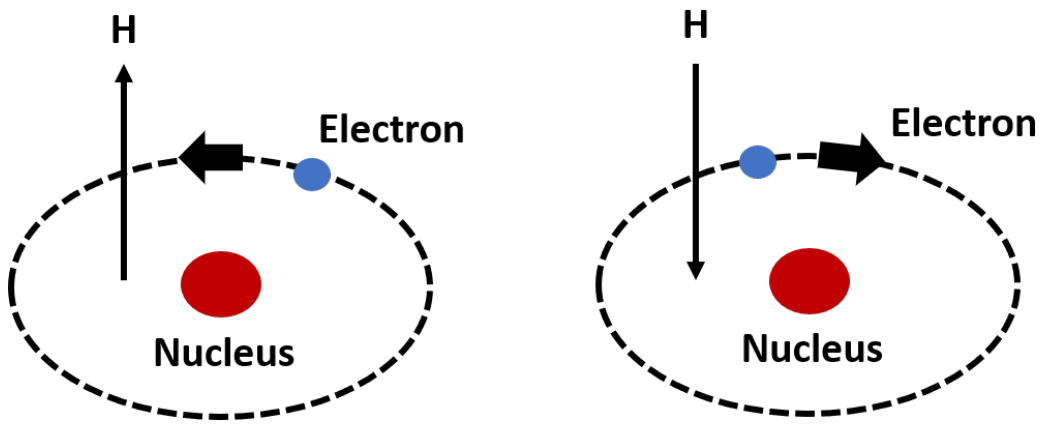

Figure 2.1: Schematic of the origin of magnetism from the electronic structure in a free atom.

netic field. The electron configuration of diamagnetic material is usually fully filled that no permanent magnetic moment could contribute to magnetization. Most transitional metal salts are paramagnetic that magnetization increases proportionally to the applied magnetic field as suggested by Curie-Weiss Law. The net magnetic moment originates from the partially filled d-shell. With a weak coupling between neighboring spins through the mediation of anions in the crystal structure, the small magnetization is perfectly reversible to its random state when applied field is removed. Graphs of M as a function of H, namely magnetization curves, are commonly used as an illustration of magnetism types of materials. In paramagnets and diamagnets, the magnetization curves are represented by a positive and negative slope respectively, both of which are reversible in dipole moment orientations, restoring its random alignments when the applied field is removed. In ferromagnetic materials, the neighboring spins are coupled and aligned in the same orientation to achieve a lower energy state. Ferromagnets become paramagnets when the temperature is elevated beyond Curie temperature, T_c. Above the critical temperature, thermal energy outweighs the coupling of spins, and thus destroying the long-range FM ordering. The importance of ferromagnets originates from their hysteresis characteristics under applied magnetic field. The magnetization increases with increasing magnetic field until reaching saturation

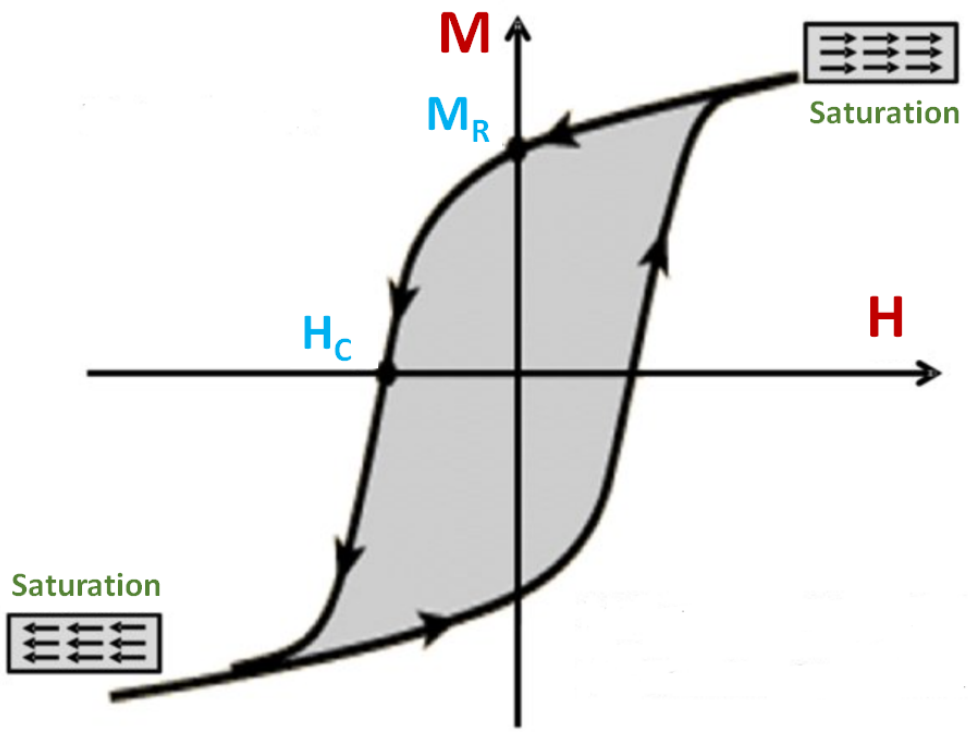

Figure 2.2: Schematic of ferromagnetic hysteresis loop.

M_s with a corresponding field H_s. Further elevation of magnetic field strength does not change magnetization value since all magnetic (Weiss) domains are aligned, reaching its maximum value. A typical hysteresis response is shown in Figure 2.2. When the applied field slowly decreases, magnetization does not follow the previous path, but a curve with higher magnetization values due to the strong coupling of domains in ferromagnets. When the applied field is removed, the intrinsic demagnetizing field rotates domains in opposite direction. However, such a field is not strong enough to overcome the exchange interactions between domains. The magnetization remains as remanence or remnant magnetization M_r. Fully demagnetization occurs at coercivity or coercive field strength H_c, which is a measure of the "hardness" of the ferromagnetic material and the energy required for demagnetization.

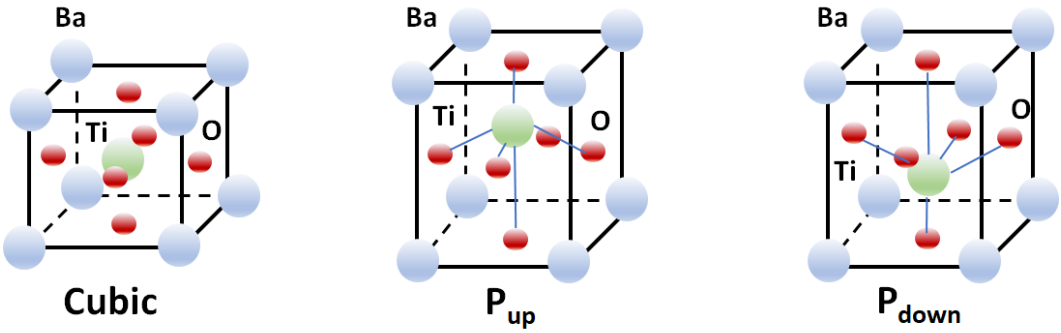

Figure 2.3: Crystal structure of the perovskite ferroelectric $BaTiO_3$ with high temperature, paraelectric, cubic phase and room temperature, ferroelectric, tetragonal phases, showing up and down polarization variants. The atomic displacements are scaled to be clearly visible.

2.2 Ferroelectricity

Just like ferromagnetism, ferroelectricity is characterized by a spontaneous polarization in the absence of external electric field. By applying external electric field this spontaneous polarization can be switched. Generally, ferroelectric materials experience a structural phase transition from a paraelectric phase to a ferroelectric phase upon cooling through the Curie temperature, T_c. Above T_c, the crystal has a centrosymmetric structure and has no spontaneous polarization. Nevertheless, below T_c, the crystal shows ferroelectricity and has a structure resulting from a change in the symmetry of the unit cell[29]. One of the well-known ferroelectric structures is the perovskite ABO_3. When a perovskite ferroelectric is below the Curie temperature, T_c, the central ion in the unit cell is displaced from its equilibrium position to create a spontaneous polarization, as shown in figure 2.3. Consequently, a perovskite ferroelectric material transforms from a paraelectric phase with a centrosymmetric structure into a ferroelectric phase with non-centrosymmetric structure which is usually even tetragonal or rhombohedral. Below the phase transition temperature, there are at least two directions along which the spontaneous polarization can exist in a stable state. The most common examples of perovskite ferroelectric materials are $BaTiO_3$ and $PbTiO_3$ [29].

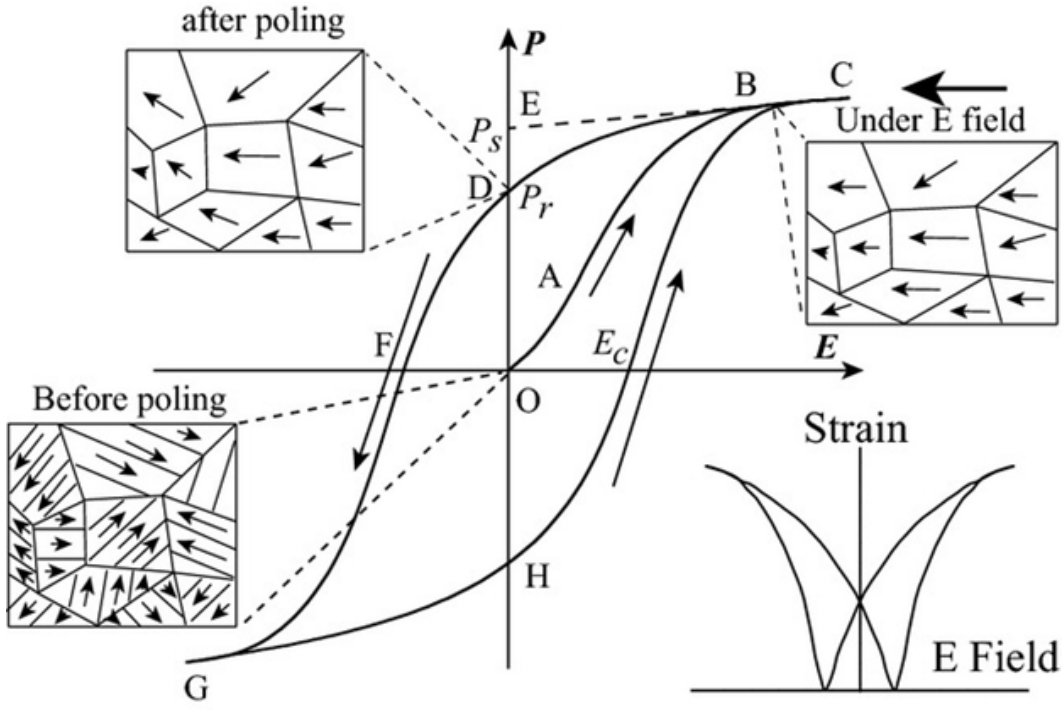

Figure 2.4: A typical hysteresis loop in ferroelectrics and corresponding domain reversal (polarization rotation) and strain–electric field curve [30].

2.2.1 Polarization switching and domain wall motion

A ferroelectric domain is a region within a ferroelectric in which the spontaneous polarization is uniformly oriented in one direction. The interface between two domains is called domain wall. When an external electric field is applied in a direction opposite to the polarization, the polarization can be reoriented in the direction of the electric field[30]. By increasing electric field, the directions of the spontaneous polarization inside domains will be forced to switch towards the field direction, resulting in a rapid increase in polarization as shown in segment OAB of figure 2.4. A saturation state is reached (BC) when all the domains are aligned parallel to the field direction. The linear extrapolation of the segment BC back to the polarization axis (CBE) represents a linear dielectric and piezoelectric response. The polarization value at point E (Ps) represents the saturated polarization, which represents the volume averaging of the spontaneous polarization of all domains. By decreasing the field strength, the polar-

ization will decrease to point D. This value is called the remanent polarization (P_r). This value is nonzero because in piezoceramics some of the domains remain aligned and the others are reoriented due to grain and domain interaction. The poled state remain until the applied field in the reversed direction reaches a certain value (at the point F in the figure). The electric field required to reduce the polarization to zero again is called the coercive field (E_c). Increasing the field again will cause an alignment of the dipoles in the opposite direction. The piezoelectric responce of the ferroelectric materials is chractrized by the butterfly shape loop of the strain vs E field as shown in fig.2.4.

2.2.2 Relaxor Ferroelectrics

Relaxor ferroelectrics (RFE) or relaxors, exhibit many properties similar to those of spin and dipolar glasses. Normally relaxor behavior in FE materials results from compositionally induced disorder or frustration[31]. This behavior has been observed and studied most extensively in disordered ABO_3 perovskite ferroelectrics and is also seen in mixed crystals of hydrogen-bonded ferroelectrics (FEs) and antiferroelectrics (AFEs), the so-called protonic glasses. Relaxor ferroelectrics are characterized by a broad maximum in the temperature dependence of the real part of the dielectric permittivity ($\epsilon^{'}$), a frequency-dependent temperature of the dielectric maximum (T_m) and a strong relaxation dispersion of the permittivity at temperatures around and below T_c [32]. In the ABO_3 oxides substituting ions with different sizes, valences, and polarizabilities at both the A and B lattice sites produces dipolar defects and can introduce a sufficiently high degree of disorder so as to break translational symmetry and prevent the formation of a long-range ordered state. In these highly polarizable host lattices, the presence of a dipolar impurity on a given site can induce dipoles in a number of adjacent unit cells within a correlation length of that site leading to the formation of polar nanodomains[33]. Indeed, such nanodomains have been observed in many ABO_3 relaxors. Two important characteristics of this relaxor state that are distin-

guished from simple dipolar glasses or spin glasses are the predominant existence of the dipolar nanodomains and the presence of some degree of cooperative freezing of the orientational degrees of freedom[34]. The existence of dipole nanoregions due to the compositionally disorder introduces a high piezoelectric coefficient. One of the most common and well-known relaxor ferroelectric materials is lead magnesium niobate – lead titanate $PbMg_{2/3}Nb_{1/3}O_3$-$PbTiO_3$ which possesses high ferroelectric and piezoelectric properties desirable for a wide varieties of applications[35].

2.3 Multiferroic and magnetoelectric materials

Recently, multiferroic materials have attracted big interest because of their large potential for applications in novel electronic devices [6, 36–41]. Multiferroics are these kinds of materials that have at least two ferroic properties in one system, with the ferroic properties including ferroelectric, (anti-) ferromagnetism, and ferroelastic. A combination of these multiple ferroic orders may provide close coupling among them, facilitate the way to realize cross-control of various ordered parameters. Strong magnetoelectric coupling can be induced due to the strong coupling interaction between two ferroic orders[38]. As shown in Figure 2.5 (a) multiferroic materials require two or all three of the properties, ferroelectricity, ferromagnetism, and ferroelasticity exist at the same phase[42]. By definition, the magnetoelectric coupling can be named as direct and converse magnetoelectric coupling. For the direct magnetoelectric coupling, there is an appearance of electric polarization by the application of a magnetic field. In this case, the external magnetic field applied on the multiferroic material has the ability to modulate the electric polarization of that material. Also, electric potential or voltage output can be induced by the applied alternating magnetic field which may lead to high-resolution magnetic field sensor applications[43]. As the same way, the converse magnetoelectric response is the induced magnetization upon the application of an external electric field. This means the modification of magnetic property by an electric

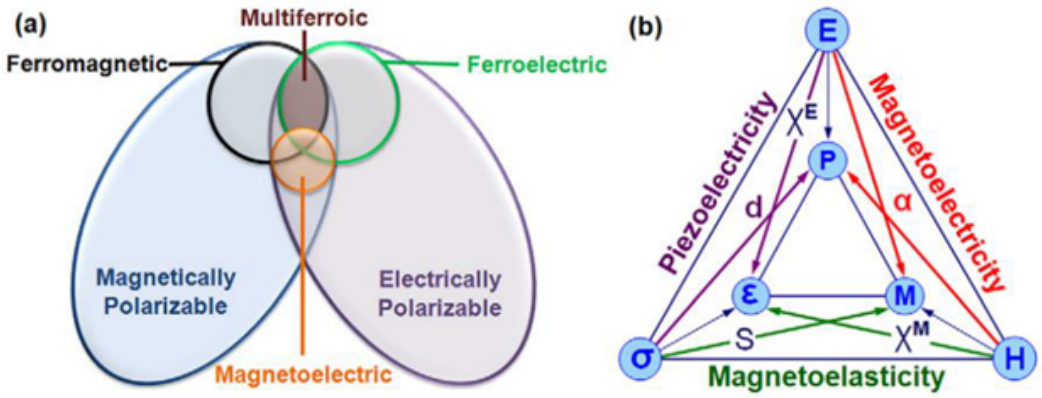

Figure 2.5: a) Relationship between multiferroic and magnetoelectric materials.(b) Schematic illustrating different types of coupling present in materials. [42].

field which provides great opportunities in the voltage control of spintronics, reconfigurable electronics, and tunable microwave devices with ultra-low energy consumption [4, 44, 45]. Multiferroic materials can be subdivided into single phase multiferroics, composites and multiferroic heterostructures as we will discuss as follows.

2.3.1 Single phase multiferroic

Single-phase multiferroic materials exist in nature or can be synthesized which display an intrinsic magnetoelectric effect. Single-phase multiferroic materials combine ferroelectric polarization and ferromagnetic or anti-ferromagnetic magnetization in the same phase [46]. Therefore, the magnetization can be controlled by the application of external electric field and likewise the ferroelectric polarization can be controlled by an applied magnetic field. However, single-phase multiferroic materials are rarely found. As proposed by Khomskii, multiferroics can be divided into two types: type-I and type-II [47]. Type-II multiferroics, in which the ferroelectricity is generated in specific magnetic ordering, are also called magnetism-driven multiferroics. Although Type-II multiferroics has the same origin of polarization and magnetism, it shows a very small polarization and small magnetoelectric constant. On the other hand, single-

phase multiferroics that do not possess a magnetic origin of ferroelectricity can be characterized as type-I multiferroics [48]. $BiFeO_3$ is the most common and well-known type-I multiferroics where ferroelectricity and magnetism are believed to originate from two different origin. The s lone pair electrons of Bi is responsible for the appearance of ferroelectricity while the 3d-electrons of Fe is responsible for antiferromagnetic (AFM) order[49]. For type-II multiferroic materials, electric polarization is believed to be generated by a specific magnetic order, allowing a remarkable ME response. It was initially discovered in orthorhombic $RMnO_3$[50] and RMn_2O_5[51], and then large number of fabricated materials showed type-II multiferroicity. Single-phase multiferroic materials have been widely studied in both bulk and film phases. In most of these materials the intrinsic magnetoelectric effect only can be found below room temperature. Strong magnetoelectric coupling above room temperature has not been found in any of these compounds, which leads to limits the practical applications of single-phase multiferroic materials. Consequently, multiferroic composites with higher design flexibility and stronger magnetoelectric coupling at room temperature have drawn significant interest in recent few years.

2.3.2 Multiferroic Composites

Because natural multiferroic single-phase compounds are very rare, and their magnetoelectric (ME) responses are also so weak or occur at too low temperatures, multiferroic composites compining both FE and ferromagnetic phases are a good choice for application point of view. They mainly display giant ME coupling responses above room temperature, which makes them ready for several technological applications. Suchtelen [52] proposed the concept of a product property in two-phase composite materials in 1972, arising from an elastic coupling between two phases of different properties. Several interesting ME composites investigated in recent years can be divided into three groups.

Bulk Ceramic Composites: The ceramic composites which consist of piezoelec-

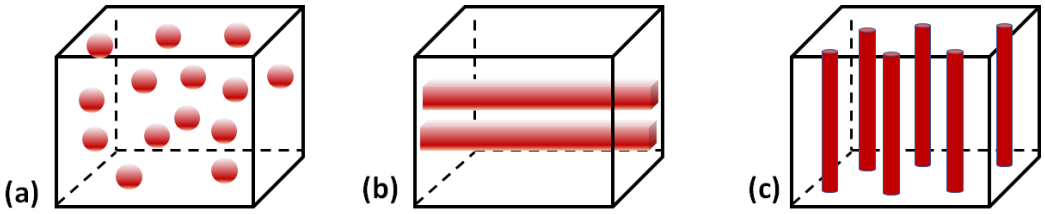

Figure 2.6: Schematic illustration of three bulk composites with the three-common connectivity schemes: (a) 0-3 particulate composite, (b) 2-2 laminate composite and (c) 1-3 fiber/rod composite.

tric and magnetic oxide ceramics are investigated. Two-phase composite is defined as 0-3, 2-2, 1-3 which can be understood using the concept of phase connectivity introduced by Newnham et al. [53]. for example, a 0-3 type ceramic composite means one-phase particles (denoted by 0 embedded in the matrix of another phase (denoted by 3). Figure 2.6 represents a schemes used commonly for designing the multiferroic ceramic composites, in which are (a) 0-3 type particulate composites of piezoelectric and magnetic oxide grains, (b) 2-2 type laminate composites of BTO based FE ceramics and ferrites, PZT and ferrites (or doped ferrites), (SrBa)NbO and ferrites, and so on [54], and (c) 1-3 type fiber composites with fibre/rod of one phase embedded in the matrix of another phase.

Two phase ME Composites of Magnetic Alloys and Piezoelectric Materials: Iron alloys and rare-earth-iron alloys are very well known for displaying much higher magnetostriction property compared to the magnetic oxide (such as ferrite) ceramics. Thus, the composites of these alloys and piezoelectric materials should have much large ME response which displayed through the strain effect.

Nanostructured Composite Thin films: Most recently, motivated by a pioneer work of Zheng et al.[49], multiferroic nanocomposite thin films consisting of ferroelectric material (such as BTO, PTO, PZT and PMN-PT) and magnetic/magnetic oxides are synthesized by thin film deposition techniques have become new routes to multiferroic composites[55]. In comparison to bulk multiferroic ME composites, the nanostructured thin film multiferroics provide more degrees of freedom, such as lattice strain or

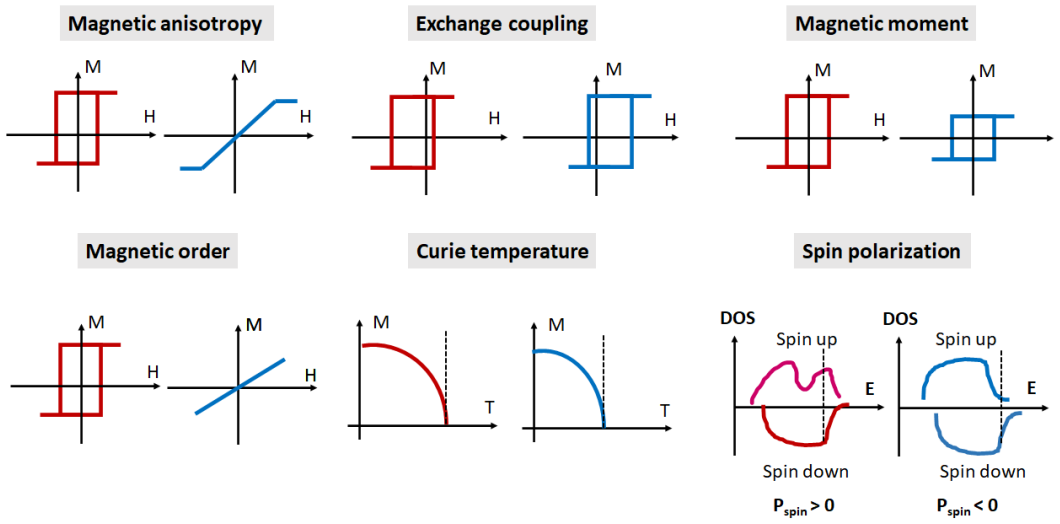

Figure 2.7: Electric field control of magnetic properties

interface interaction, to enhance the ME behavior.

2.4 Electric field control of magnetism and magnetoelectric effect

One of the most important features of multiferroic materials is the coexistence of coupling interaction between two ferroic phases. For example, the coupling between ferroelectric and ferroelastic phases can generate piezoelectricity. As well coupling between the ferromagnetic and ferroelastic phases can produce magnetostriction. Also, the coupling between the ferromagnetic order and ferroelectric phases can produce new magnetoelectric devices used in a wide variety of applications [56]. Generally, the magnetoelectric effect is created by a coexistence of the ferroelectric phase and the ferromagnetic phase in the multiferroic material (or structure). For example, the application of a magnetic field can control the electric polarization through the direct magnetoelectric effect (DME). As the same way, an applied electric field can modulate the magnetization through the converse magnetoelectric effect (CME). We will discuss next the effect of electric field on the magnetic properties of multiferroic structure.

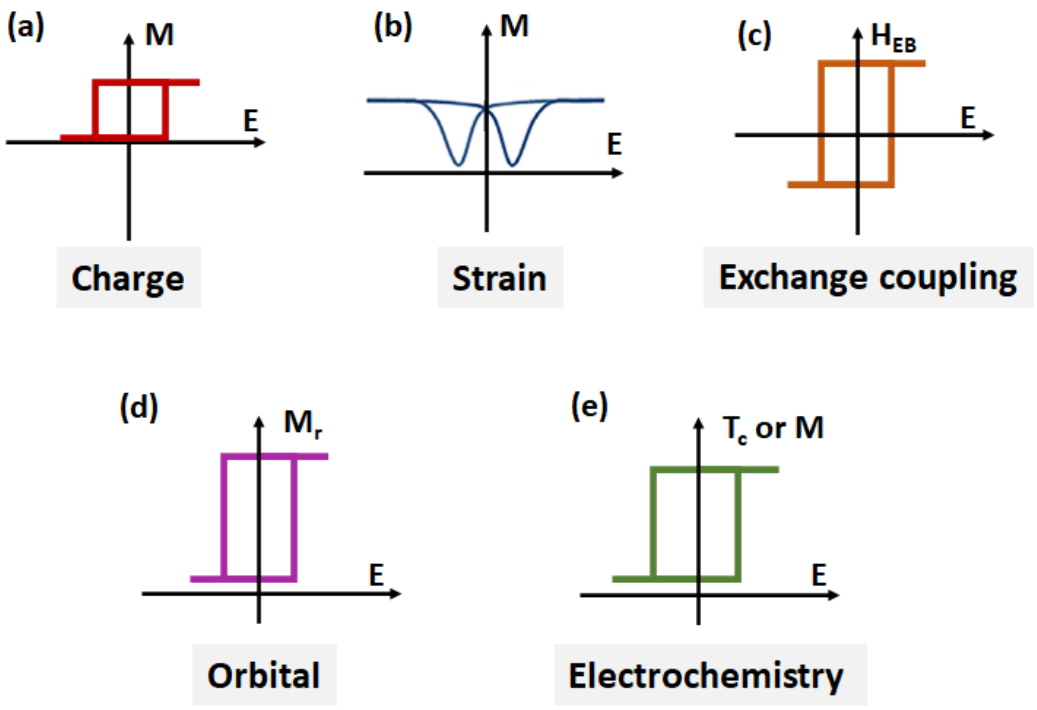

Figure 2.8: Schematic of the different magnetic responses to an electric field in heterostructures with different mechanisms: (a) charge, (b) strain, (c) exchange coupling, (d) orbital, and (e) electrochemistry

There are different ways that the electric field can affect the ferromagnetic properties of the multiferroic structure, which consequently demonstrates the possibilities of applications of material with magnetoelectric coupling. Fig 2.7 shows some examples of electric control of magnetic properties. As shown from the figure we can realize the E field modulation of magnetic properties as a change in magnetic anisotropy, exchange coupling/biase, magnetic moment and also the change in the magnetic order or even the change in the density of states of the ferromagnetic phase[57].

2.5 Mechanisms under voltage control of magnetism

The main mechanisms for the voltage modulation of magnetism depend on several parameters. For example, the selection of magnetic and piezoelectric materials, the thicknesses of the films, the crystal orientations of both FM and FE materials, and the

operational mode of the electric field. So, there are many possible mechanisms can be responsible and cooperates for ME coupling primarily due to the diversity of factors that mentioned above[58]. The most common mechanisms are divided into five types that are, carrier modulation, strain effect, exchange coupling, orbital reconstruction, and electrochemical effect. Among them, the first three mechanisms are the most common mechanisms referring to charge, lattice, and spin degrees of freedom, respectively, which are usually used to explain the origin of voltage control of magnetism phenomena. As a result of these mechanisms, various magnetic behaviors such as magnetic anisotropy, magnetization intensity, exchange bias, magnetoresistance, and Curie temperature can be manipulated as shown in Fig 2.8. Here is a small introduction to the first three mechanisms.

2.5.1 Strain mediated coupling

This arises commonly from an elastic coupling between ferromagnetic and ferroelectric material. For example, in the case of the application of electric field, it produces strain due to the piezoelectric property of the ferroelectric phase. This strain affects the ferromagnetic properties through the magnetostriction effect of the ferromagnetic phase[59–62].

2.5.2 Charge mediated coupling

The coupling occurs due to the ferroelectric accumulation of charges at the interface in the case of multiferroic heterostructures. Therefore, the change in these interfacial charges would induce changes in the magnetic properties[19, 63, 64].

2.5.3 Exchange bias mediated coupling

The exchange coupling or exchange bias effect is mainly observed at the interfaces between ferromagnets and antiferromagnets heterostructures, reflected by a shift of the

magnetization curve away from the origin[65, 66]. Mainly, the origin of the exchange bias is the pinning of the domain walls of the antiferromagnetic phase. Due to the coupling between the ferroelectric and the antiferromagnetic domains, the application of the electric field changes the ferroelectric domain configuration which is converted to magnetization changes[67].

Chapter 3

Experimental and measurement methods

In this chapter, we will explain the details of our heterostructures fabrications. Also, we will describe the experimental techniques used to characterize the structures and measure the magnetoelastic and magnetoelectric coupling of our multiferroic heterostructures.

3.1 Material fabrication

3.1.1 Magnetron sputtering system

Magnetron sputtering technique is considered as one of the most useful deposition methods[68]. The metals are deposited with a strong and uniform adhesion without any change in the composition. The mini/multi sputtering machines were used to deposit FeSiB amorphous films with different thicknesses and the ferromagnetic multilayer heterostructure with the composition of CFB/Pt/NiFe using the DC sputtering mechanism with a power of 500W. Figure 3.1 shows a photograph of the mini sputtering system.

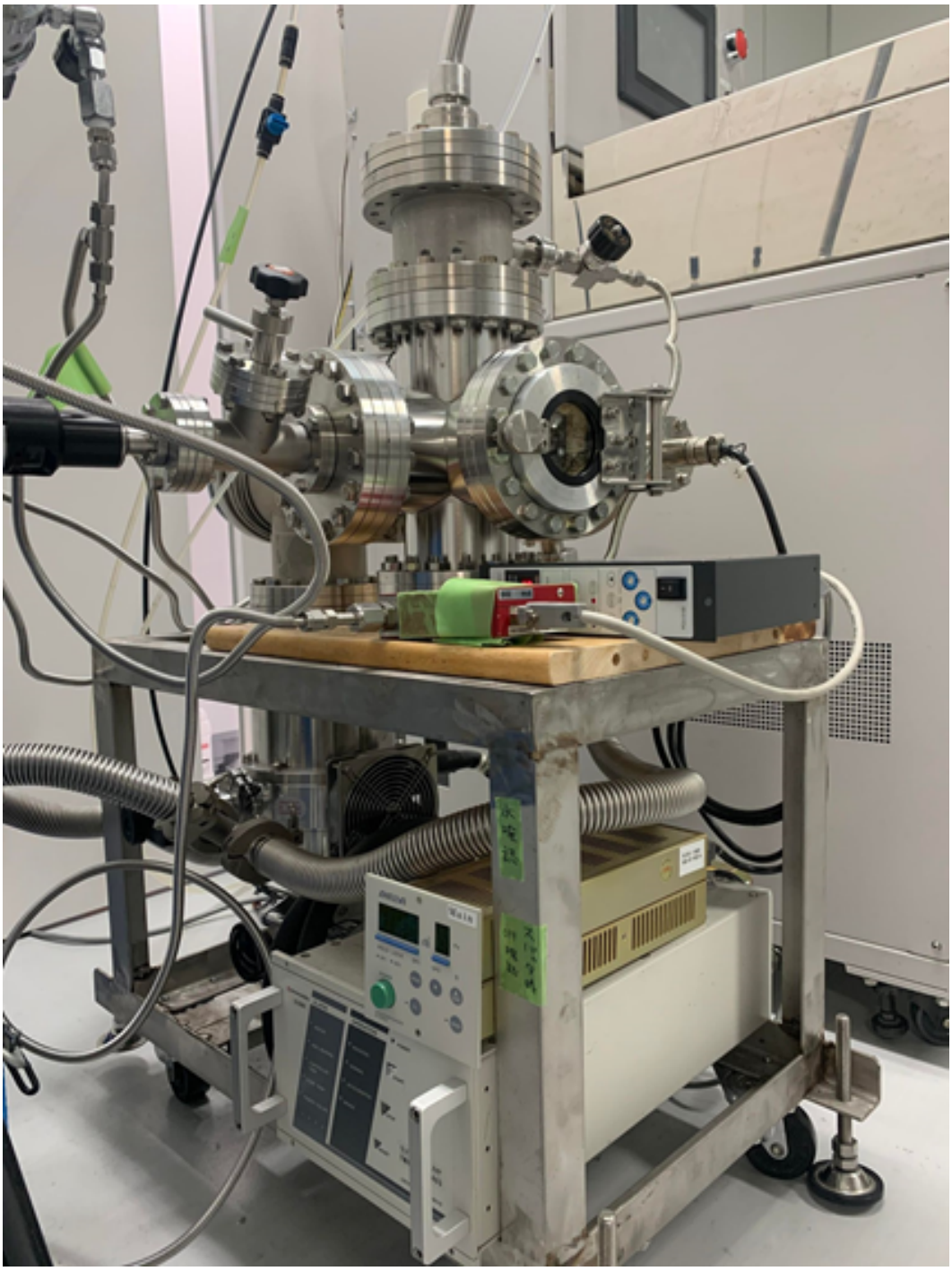

Figure 3.1: Photograph of our sputtering system.

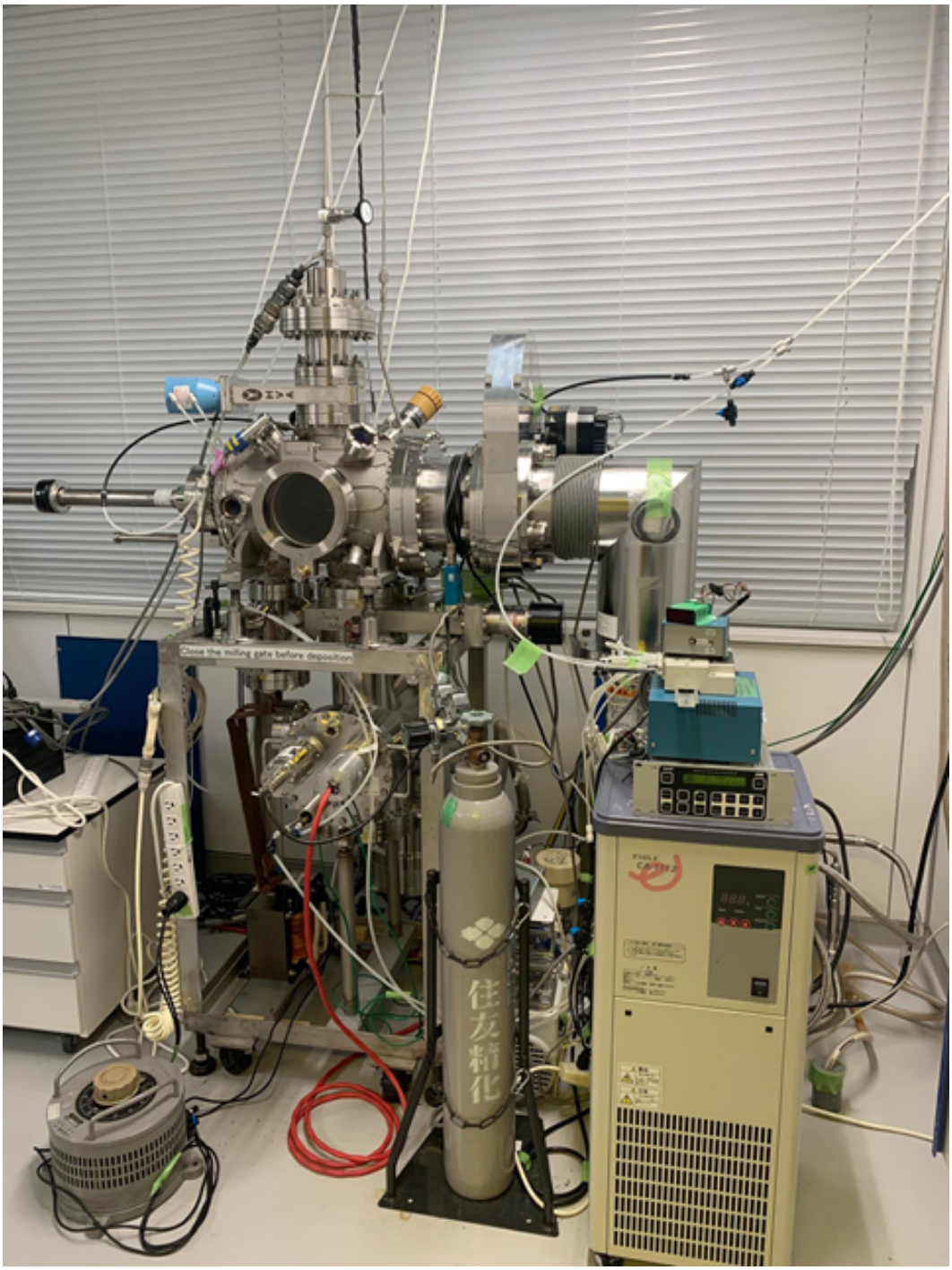

Figure 3.2: Photograph of Joule-heating deposition system.

3.1.2 Joule-heating evaporation system

The joule-heating evaporation system is a metal-deposition method, in which a target metal is evaporated through Joule heat and deposited on the sample. The joule-heating evaporation system was used mainly to deposited copper electrodes to the studied multiferroic heterostructures.

3.2 Structural and Surface Morphology Characterization

The crystal structure and the surface morphology of the prepared samples were characterized using X-Ray diffraction (XRD) and atomic force microscopy (AFM). Also, X-ray photoelectron spectroscopy (XPS) was used to analyze the chemical elements and bonding of the sample surfaces and to study the heterostructures interface regions before and after E field application.

3.2.1 X-Ray diffraction (XRD)

The crystal structure of the prepared samples was determined by the X-ray diffraction technique. A BRUKER D8 ADVANCE Diffractometer operated at 40 kV and 40 mA with a wavelength of 1.5406Å (CuKα) was used. The basic law involved in the diffraction method of structural analysis is Bragg's law. When monochromatic X-rays hit upon the atoms in a crystal lattice, each atom acts as a scattering source. The crystal lattice acts as a series of parallel reflecting planes[69]. The intensity of the reflected beam at certain angles will be maximum when the path difference between two reflected waves from two different planes is an integral multiple of as shown in Fig. 3.3. This condition is termed as adjacent Bragg's condition and is given by the relation:

$$2dsin\theta = n\lambda \tag{3.1}$$

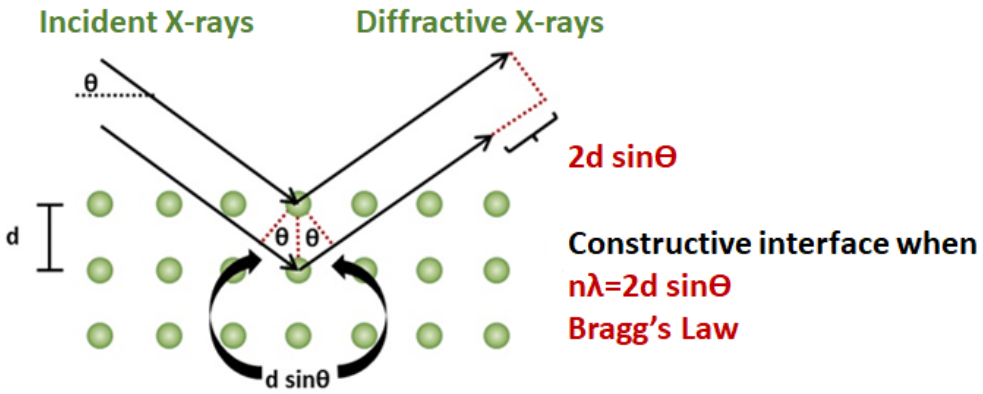

Figure 3.3: Schematic illustration of XRD.

where n is the order of diffraction, λ is the wavelength of the X-rays, d is the spacing between consecutive parallel planes and θ is the diffraction angle. From X-ray diffraction pattern we can estimate the crystal structure and orientations, the sample composition, and different types of phases appearing in the material. We also evaluate the average crystalline size from the width of the peak in a particular phase pattern. X-ray diffraction pattern is also considered as an analysis of structural distortion arising from the variations in d-spacing caused by the strain[70].

3.2.2 X-ray Photoelectron Spectroscopy (XPS)

X-ray photoelectron spectroscopy (XPS) or electron spectroscopy for chemical analysis (ESCA) is a technique that analyzes the elements composition and its chemical bonding state at the sample surface and interfaces[71]. The main technique is irradiating x-rays on the sample surface and measuring the kinetic energy of the photoelectrons emitted from the sample surface or interfaces. XPS instrument can obtain information on elements within a few nanometers of the sample surface. Additionally, the change in bond energy (chemical shift) caused by the electron state surrounding the atoms to be analyzed, such as atomic valence charges and interatomic distances, tends to be greater than the chemical shift observed in Auger electron spectroscopy (AES), which makes the relative ease with which the state of chemical bonds can be identified another

advantage of XPS[72]. XPS spectra were obtained using a PHI 5000 VersaProbe III Photoelectron Spectrometer with monochromatic Al Kα X-ray radiation (1486.6 eV). We can say that the XPS technique is an important tool for studying the E field modulation of the multiferroic heterostructure interfaces.

3.2.3 Atomic force microscopy (AFM)

AFM is a very high resolution type of scanning probe microscope which is considered as a powerful technique to measure and observe the topography of the sample on the nanoscale range[73]. In AFM the information about the sample topography is collected by the interaction between the surface of the sample and the mechanical probe during the measurement. Here the probe has a very tiny and sharp tip attached to the end of a cantilever. The cantilever can be made of single-crystalline silicon or silicon dioxide. There are two main methods for measuring the force between the surface and the probe. One is the contact mode in which the tip is directly in contact with the sample surface, and the interaction force is dominated by Van der Waal's interaction[74]. The other mode is the tapping mode which is a non-contact mode. A drive signal is applied by a piezoelectric crystal with typical frequencies to the "Tapping Piezo", which mechanically oscillates the probe at its resonance frequency. The interaction between the tip and the sample surface changes the cantilever oscillation amplitude or the phase relative to the drive signal. We used AFM technique to study the surface morphology of our heterostructures.

3.3 Measurements methods

3.3.1 Vibrating Sample Magnetometer

Room temperature magnetic hysteresis (M-H) loops of our heterostructures were measured by vibrating sample magnetometer (VSM). The sample is placed between the

poles of an electromagnet with a uniform magnetic field as shown in Fig. 3.4. The main driving mechanism is that the sample undergoes mechanical vibrations that induce a change in the magnetic flux[75]. Then the magnetic flux change induces a voltage in the pickup coils. The magnetic moment of the sample is measured after careful calibration of the VSM with a standard sample. The amount of the electrical signal in the picked-up coil is proportional to the frequency and amplitude of the vibration of the sample, and the magnetic moment of the sample at the applied magnetic field. The frequency and amplitude of the vibration of the sample are kept constant by the reference capacitor. After the calibration of the VSM with the standard sample, the magnetic moment of the sample is measured. M-H loops also were measured under the application of bipolar electric field. Copper wires were connected to the measured samples by silver paste electrodes and up to 14 kV/cm E-field was applied.

3.3.2 High Voltage Set-Up for the Converse ME effect

To study the converse ME coupling effect, a high E field (a maximum of 14 kV/cm) was applied to the piezoelectric PMN-0.3PT substrate so that a large strain was created in the sample. Then the effect of the strain on the magnetic properties of the thin films was investigated. Therefore, for this measurement, a high voltage setup was built up within the VSM system. As shown in Fig.3.5, the H-field was applied along the in-plane direction of the PMN-0.3PT, while the E field was applied along with the out of plane direction of the sample.

3.4 Ferroelectric Hysteresis Loop or P-E Loop

The dielectric polarization as a function of electric field was measured using Sawyer-Tower (S-T) circuit as shown in Fig.3.6. The S-T circuit is considered as a practical circuit for the characterization of ferroelectrics and studying fundamental phenomena such as spontaneous polarization, remnant polarization, coercive-field, and polarization

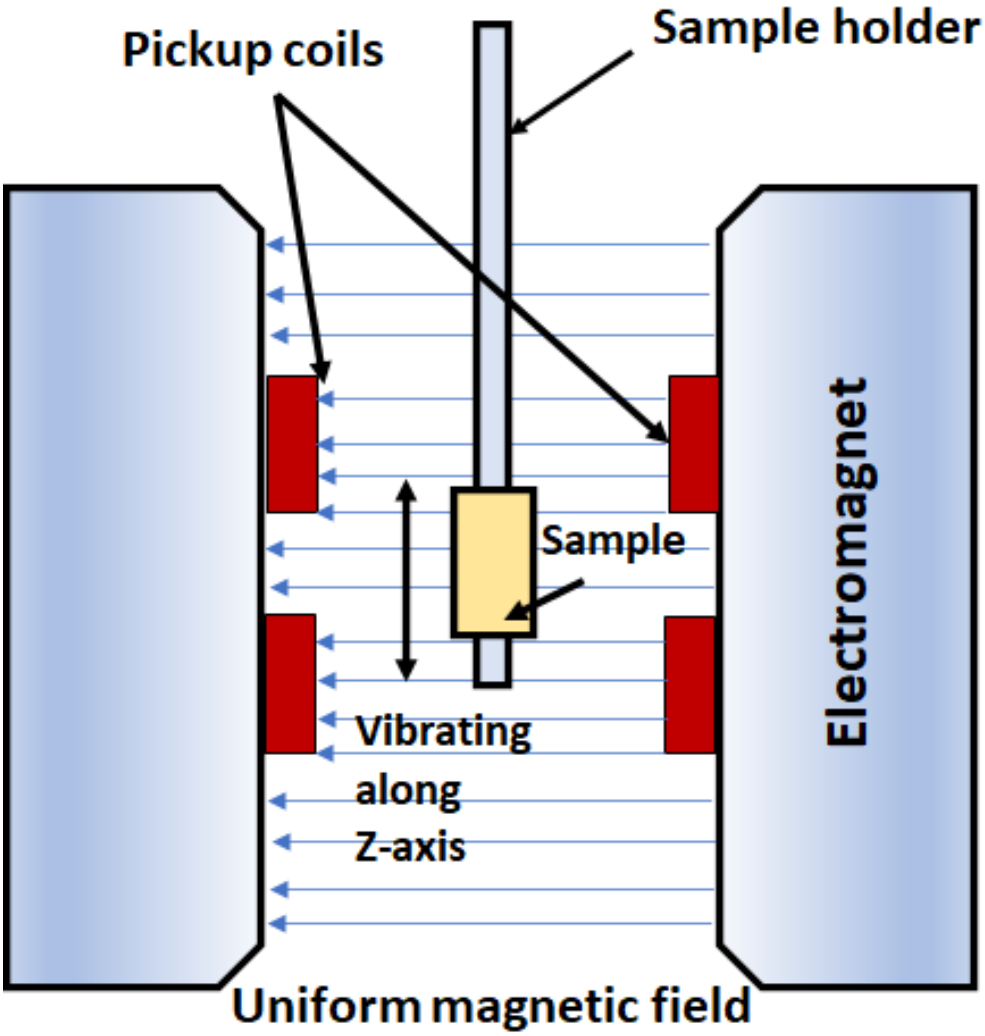

Figure 3.4: Schematic illustration of VSM.

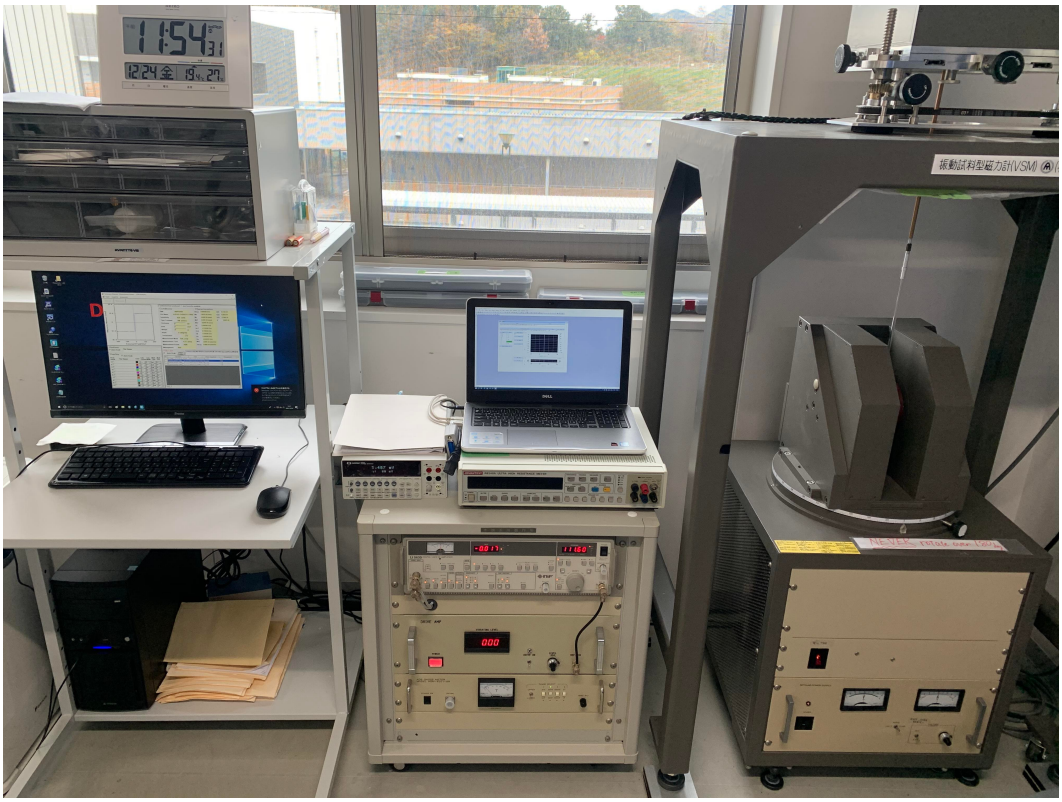

Figure 3.5: our M-E measurement setup.

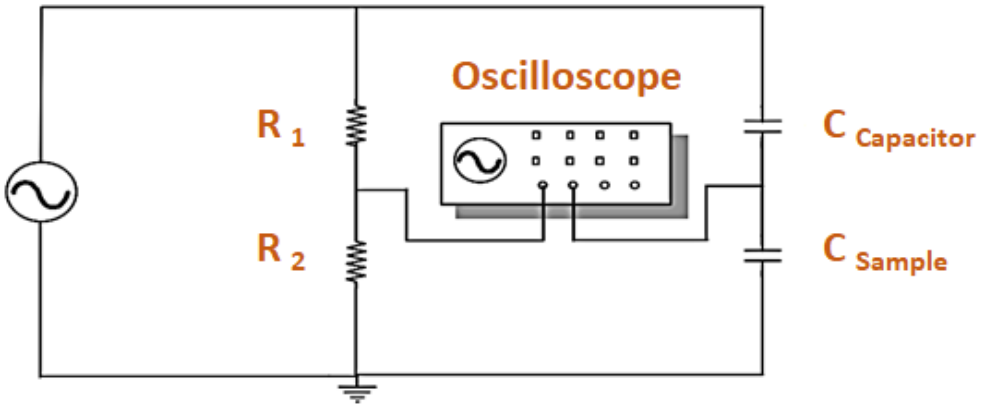

Figure 3.6: Schematic illustration of Sawyer-Tower circuit.

reversal mechanisms[76]. The circuit mainly consists of two capacitors, one due to sample (C_s) and the other one is a linear capacitor with a well-known value (C_c). They are in series, where C_c is chosen much greater than C_s so that voltage drop across C_c is much smaller than that across C_s (sample). So the drive voltage V_d is almost equal to voltage across C_s. The voltage across C_s, which gives polarization of the sample, is applied to vertical plates of the oscilloscope, and the drive voltage after safe attenuation is applied to horizontal plates of the oscilloscope to measure the electric field across the sample.

3.4.1 Ferromagnetic resonance experiment

FMR absorption is an interesting resonance phenomenon that occurs when a constant magnetic field and a microwave field are applied to a ferromagnetic specimen simultaneously, and the resonance conditions are satisfied[77]. FMR is mainly defined by a uniform precession of the magnetic moments of the material around the effective applied field. The conventional method to measure FMR is to keep the microwave frequency constant and vary the magnetic field. At some field the resonance occurs. Here in our multiferroic heterostructures, the magnetization dynamics have been evaluated by measuring the derivative ferromagnetic resonance (FMR) spectra before and after the application of E field. The measurement system for the derivative FMR has been developed by the broadband power transmission system based on the coplanar waveguide under the external magnetic field. The E field modulation of the FMR spectra gives us clear information about the magnetoelectric coupling mechanisms.

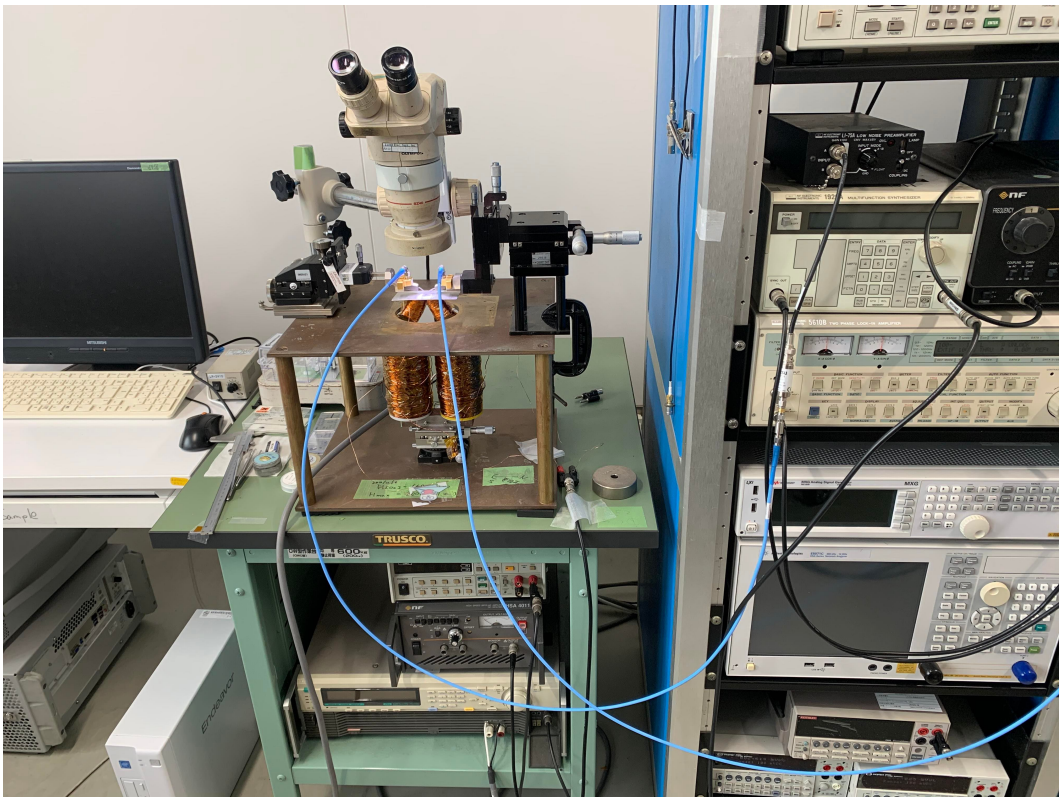

Figure 3.7: Our FMR system

Chapter 4

Modulation of magnetic anisotropy in FeSiB film sputtered on curved substrate

4.1 Introduction

Functional magnetic and/or spin devices such as magnetic sensor, storage and memory are driven by manipulating and stabilizing the magnetization of ferromagnets like the modulation of magnetic anisotropy[78–81]. Magnetic anisotropy is mainly caused by the symmetry of the crystal structure. Applying magnetic field during the annealing or the deposition is also known to induce the magnetic anisotropy[82]. In addition, in the thin film cases, the compressive or tensile strain from the substrate is also able to induce the uniaxial magnetic anisotropy through the magneto-striction effect[83].

On the other hand, flexible electronic devices based on plastic substrates have attracted considerable attention owing to its wide range of application such as health care and energy harvesting devices[84]. Since the plastic sheet is highly stretchable, significant magnetic anisotropy can be induced in the magnetic thin film prepared on the plastic sheet[85]. So, we used a Polyimide sheet as a substrate. In ferromag-

netic/polyimide sheet hybrid systems, most of the reports studied the modulation of the anisotropic magnetic constant by bending the substrate after the film deposition[25]. According to reports, the magnetic anisotropy is mainly induced by the magnetic field during the deposition and the change of the anisotropic constant due to the sheet bending was discussed. In such cases, since the magnetic field is not perfectly parallel to the film plane, the additional magneto-static interaction is induced, resulting in the unfavorable property with the necessity of the complicated analysis. In order to prevent such geometrical problems, the amorphous ferromagnetic thin films deposited on the pre-bent polyimide sheets have been used[86]. The induced magnetic anisotropy has been tuned by the curvature of the polyimide sheets during the deposition. However, the induced magnetic anisotropy is not sufficiently large because of the material properties. Here, we focus on the FeSiB, which is one of the representative magnetostrictive materials.

4.2 Samples preparation and characterization

FeSiB film with a thickness of 20 nm has been deposited on top of 50 um thick polyimide sheet by the magnetron sputtering system under the base pressure of 2×10^{-5} Pa. Here, we have optimized the distance between the target and sample in order to obtain better performance. The deposition rate of the FeSiB film is as slow as 0.1 nm/s in order to avoid the formation of contamination. The FeSiB film has been deposited on the bent polyimide sheet with a 5 mm $\times$ 10 mm rectangular shape. As schematically shown in Fig. 4.1, the curvature C of the sheet has been varied from 0.15 mm^{-1} to +0.15 mm^{-1} by changing the mold shape. After the film deposition, the magnetic properties of the FeSiB films have been evaluated under the flat-sheet condition. We have evaluated the surface roughness of the sputtered film by using atomic force microscope (AFM). For the comparison, the surface roughness for the similarly sputtered film on FZ-Si substrate has been also evaluated. Figures 4.1(b) and (c) show the AFM images of the

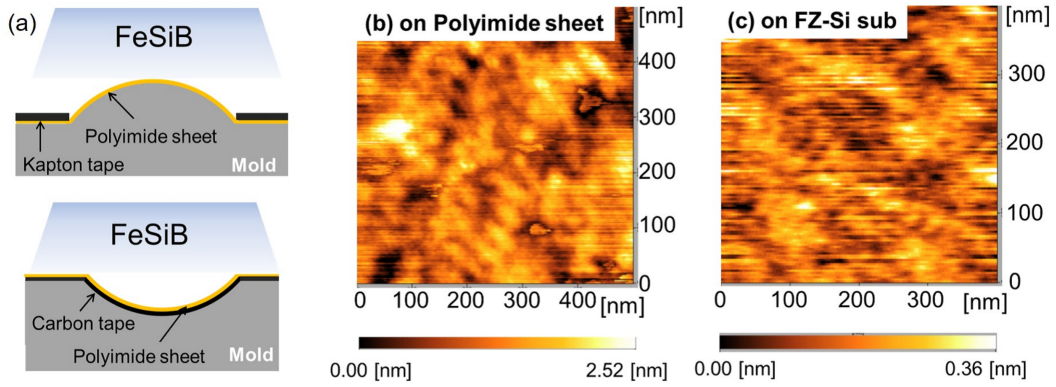

Figure 4.1: (a) Schematic illustrations of the film deposition process on the curved polyimide sheet using convex and concave molds. AFM image of the FeSiB films deposited on the polyimide sheet(b) and FZ-Si substrate (c).

FeSiB films deposited on the polyimide sheet and FZ-Si substrate, respectively. The average radius (R_a) and the root mean square (RMS) for the polyimide-sheet sample are 22.5 nm and 1.5 nm, respectively. These values are larger than those for the Si-substrate. sample, but are comparable with or better than the conventional magnetic thin films grown on the Si substrate. In addition, the saturation magnetization M_s for the FeSiB on the polyimide sheet is approximately 1.45 T, which is almost the same as that on the Si substrate. These results indicate that our prepared FeSiB film on the polyimide sheet has a moderate property.

4.3 Results and discussion

4.3.1 Magnetic properties of the non-bent sample

Here we will focus on the magnetic property of the FeSiB film. First, we evaluate the magnetic isotropy of the non-bent sample. Figure 4.2(a) shows the magnetization curves (M-H curve) under the magnetic field along the longitudinal (0 deg) and transverse (90 deg) directions. Both results exhibit typical M-H loops for soft magnetic materials with a coercive force of around 20 Oe. We emphasize that two M-H curves do not show a clear difference, implying no magnetic anisotropy. To confirm more

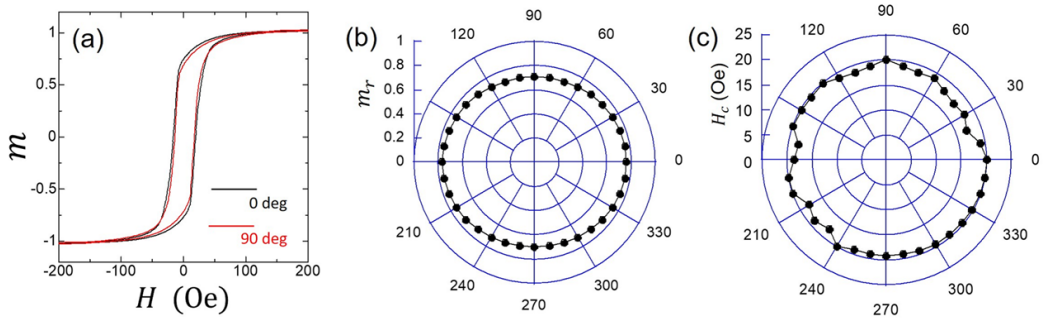

Figure 4.2: (a) M-H curves under the longitudinal and transverse magnetic fields measured by VSM. Angular dependence of the normalized remnant magnetization mr (b) and the coercive field Hc (c).

clear evidence, we investigated the angular dependence of the normalized remanent magnetization m_r and the coercive field H_c. Figures 4.2(b) and (c) are, respectively, the remanent magnetization m_r and the coercive field H_c as a function of the direction of the magnetic field. Both results clearly indicate the isotropic angular dependence, meaning that the FeSiB prepared on the flat polyimide sample has no anisotropy. Here, we emphasize that the FeSiB prepared on the Si substrate with the same recipe shows a small uniaxial anisotropy and smaller coercive force with 10 Oe. This means that the moderate surface roughness due to the polyimide-sheet sample compensates the uniaxial anisotropy[87].

4.3.2 Magnetic properties of the pre-bent samples

Here, we focus on the influence of the curved substrate on magnetic anisotropy. The magnetic anisotropy due to the pre-bent sample with the curvature C = 0.127mm^{-1} was evaluated by the M-H loops with changing the direction of the magnetic field. In this case, the compressed strain is induced during the M-H loop measurement, as shown in Fig.4.3(a). Figure 4.3(b) shows the M-H loops along with the longitudinal and transverse directions. A rectangular hysteresis with the H_C = 50 Oe was clearly observed in the transverse M-H loop, while the M-H loop along the longitudinal direction shows a gradual increase with the magnetic field with the saturation field over

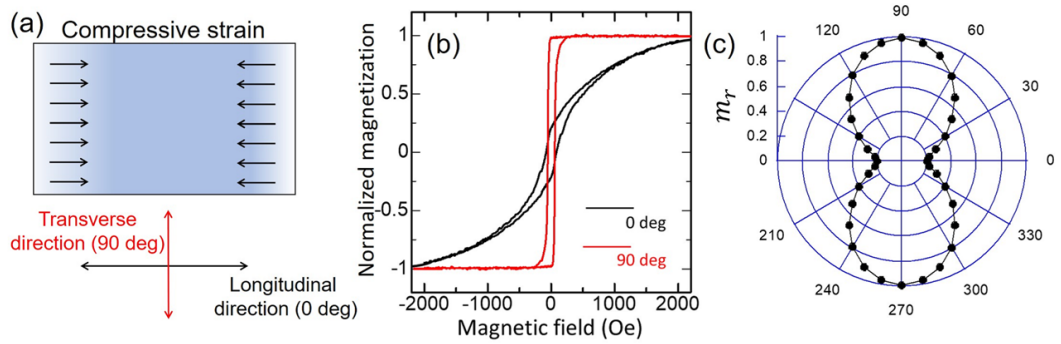

Figure 4.3: (a) Schematic illustration of the FeSiB film under the compressed strain. (b) M-H curves of the compressed FeSiB film under the longitudinal and transverse magnetic fields. (c) Angular dependence of the normalized remnant magnetization mr

2000 Oe. These results indicate that the longitudinal and transverse directions are hard and easy axes, respectively. The angular dependence of the normalized magnetization clearly indicates the uniaxial anisotropy. From the difference between the saturation magnetic field along the easy and that for the hard axes, the anisotropic magnetic constant can be estimated as 0.130 MJ/m^3. This is much larger than the value reported in CoFeB, indicating the advantage for the use of the magnetostrictive materials[88]. Thus, a large magnetic anisotropy was significantly induced in the FeSiB deposited on the convex substrate.

We then investigated the magnetic anisotropy with the negative curvature C = -0.15 mm^{-1} using the concave substrate. In this case, the tensile strain is induced along the longitudinal direction, as shown in Fig. 4.4(a). Figure 4.4(b) shows M-H loops along the longitudinal and transverse directions. In the present case, the longitudinal direction becomes an easy axis, which is opposite to the sample with the positive curvature. The estimated anisotropic magnetic constant can be estimated as 0.146 MJ/m^3, which is more efficient than that for the positive curvature. This means that the anisotropic magnetic constant changes from the positive to negative values by the sign change of the curvature. Since the magneto-striction coefficient for the FeSiB is positive, these results can be understood by the inverse magneto-striction effect[89].

Finally, we summarize the magnetic anisotropy for various curvatures. Figure 4.5

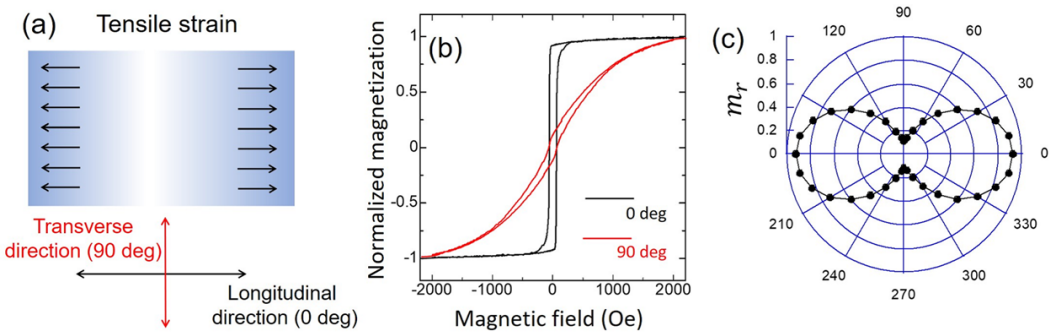

Figure 4.4: (a) Schematic illustration of the FeSiB film under the tensile strain. (b) M-H curves of the FeSiB film with the tensile strain under the longitudinal and transverse magnetic fields. (c) Angular dependence of the normalized remnant magnetization mr

shows the anisotropic magnetic constant as a function of the curvature. The anisotropic constant systematically changes with increasing or decreasing the curvature. Surprisingly, the large magnetic anisotropy accompanying with no deterioration can be induced. In addition, the sign reversal of the anisotropic constant has been achieved by changing the curvature sign. These results indicate that the combination between the magneto-striction and flexible substrate provides the efficient modulation of the magnetic property. We also investigate the coercive force along the easy axis as a function of the curvature. The coercive force increases with increasing the curvature. Since the magnetization reversal process along the easy axis is caused by the domain wall propagation, this results indicate the pinning potential for the domain wall increase with increasing the strain[90].

4.4 Summary

In summary, we have developed the FeSiB film deposition technique on the curved polyimide sheet. Although the conventional soft magnetic property has been confirmed in the FeSiB deposited on the flat polyimide sheet, the systematic change of the magnetic anisotropy was obtained by changing the curvature during the deposition. The significant magnetic anisotropy around 0.15 MJ/m^3 was found to be induced by using

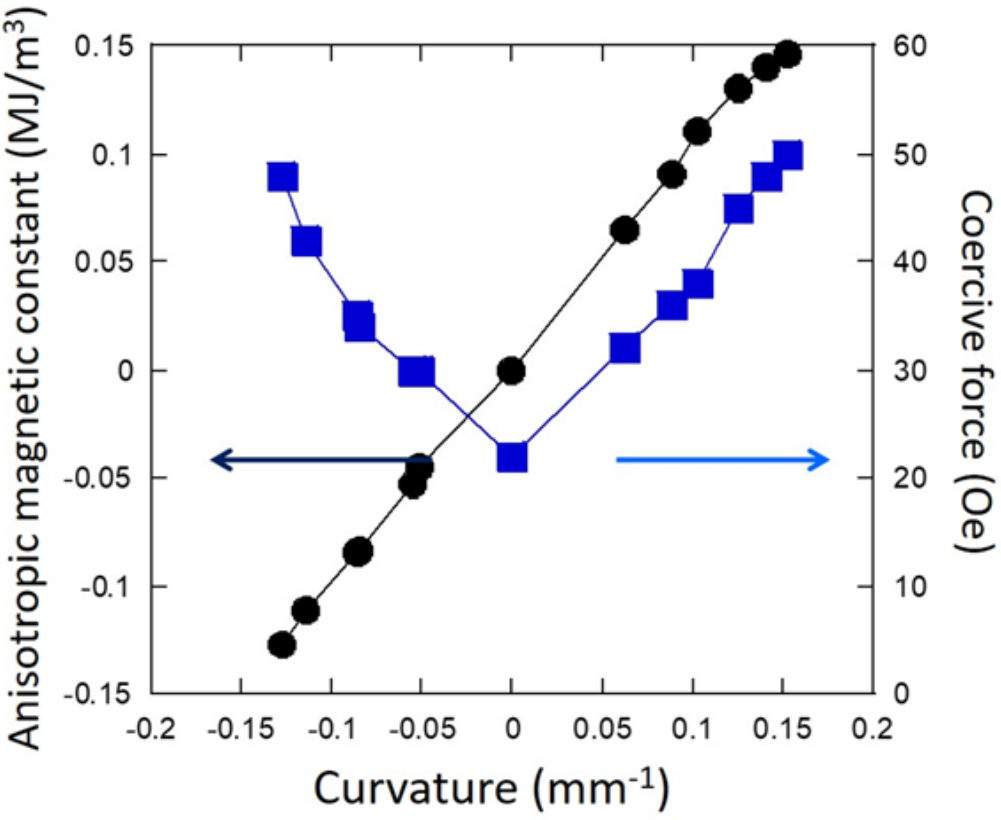

Figure 4.5: Strain-induced anisotropic magnetic constant and coercive field as a function of the curvature of the polyimide film during the deposition.

the curved sheet with the curvature of 0.15 mm^{-1}. These results indicate that the combination between the magneto-striction and flexible substrate provides the efficient modulation of the magnetic property.

Chapter 5

Thickness-dependent E field-modulated magnetism in FeSiB/PMN-0.3PT heterostructure

5.1 Introduction

Controlling magnetic properties like anisotropy or magnetization direction in a magnetic system by the application of electric field i.e. the converse magnetoelectric (ME) effect has become a prominent subject in the fields of spintronics and multiferroics[36, 91–93]. It can deliver a quick and extremely energy-efficient way for tunning magnetism compared with the traditional way of using external magnetic fields or spin currents[94]. On the other hand, such electric field tunning of magnetism can be realized by the induced ME coupling effect at the interface region of multiferroic heterostructures which artificially combines magnetoelastic magnet and piezoelectric/ferroelectric (FE) multiferroic phases. We can realize the modulation of magnetism by E-field on multiferroic heterostructures is governed by the cooperation of specific mechanisms. The strain-driven converse ME coupling[37, 95], exchange bias [96, 97], or interfacial charge-driven ME effects [98, 99]. Between them, the strain-mediated converse ME effect is gener-

ally the main driving force especially in thicker ferromagnetic film, while the other mechanism like the charge-mediated is more efficient at lower film thicknesses[58, 100].

In this chapter, the effect of magnetic layer thickness on magnetoelectric (ME) coupling in FeSiB/PMN-0.3PT heterostructures was investigated over different thickness ranges from 10 nm to 100 nm. FeSiB film was chosen to be the ferromagnetic (FM) layer due to its excellent soft magnetic properties, relatively high magnetostriction and large saturated magnetization. The PMN-0.3PT was chosen as the ferroelectric (FE) substrate due to its large piezoelectric properties especially around the morphotropic region. 100-oriented PMN-0.3PT single crystal substrate was used to study the effect of the orientation and ferroelectric domain structure on the ME properties. The results showed coexistence at room-temperature of two magnetoelectric (ME) mechanisms, i.e., strain- and interface charge-mediated couplings. The interaction between the different ME couplings leads to a remarkable thickness-dependent voltage modulation of the magnetic behavior.

5.2 Sample Preparation and characterization

FeSiB films of 10 nm, 20 nm, 50 nm, and 100 nm thickness were deposited on one side-polished unpolarized commercial ferroelectric (100)- oriented single crystal PMN-0.3PT substrates with the dimensions of 5 $\times$5 $\times$0.5 mm^3. The deposition was held by DC sputtering technique at room temperature using a FeSiB target without an applied external magnetic field as shown in Fig.5.1(a). The base pressure of the chamber was kept lower than 2 $\times$ 10 $^{-5}$ Pa, and the work power was set to 500 W. During the sputtering process, argon gas was used as the ambient gas at a flow rate of 10 sccm, and a working pressure of 0.2 Pa. Figure 5.1 (b) shows a schematic illustration of our multiferroic heterostructure. The amorphous nature of FeSiB film was confirmed by the X-ray diffraction as shown in Fig.5.1(c) in which all diffraction peaks correspond to the single crystal PMN-PT substrate. The thicknesses of the films were measured by

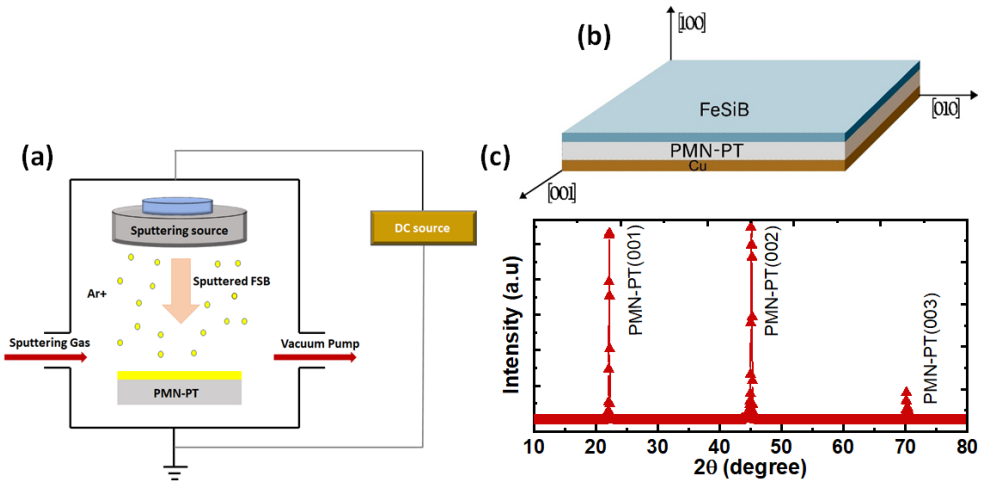

Figure 5.1: (a) Schematic illustration of film deposition. (b) Schematic illustration of the prepared MF heterostructure. (c) XRD for the 10 nm FeSiB/PMN-0.3PT.

step profiler (American Electric Power Co., NanoMap-500253PS). Polarization versus electric field (P-E) loop was measured using Sawyer -Tower circuit at a maximum electric field of 8 kV/cm to confirm the ferroelectric properties of the substrates. Silver paste and Cu wires were used for electrical connections in a two-probe configuration for the voltage dependent measurements. The static and dynamic magnetic properties and the magnetoelectric coupling were measured at room temperature using a vibrating sample magnetometer (VSM) and broadband FMR with an electric field applied across the sample thickness.

5.3 Results and discussion

5.3.1 Ferroelectric properties

Figure 5.2 (a) shows the ferroelectric hysteresis loop of (100)-oriented PMN-0.3PT single crystal with silver past as a lower and upper electrode, which demonstrates the ferroelectric property of PMN-0.3PT single crystal near morphotropic phase boundary (MPB). As shown from the figure, the ferroelectric hysteresis loop exhibits asymmetric behavior with E_c around 2 kV/cm with saturation around 6 kV/cm. This asymmetric

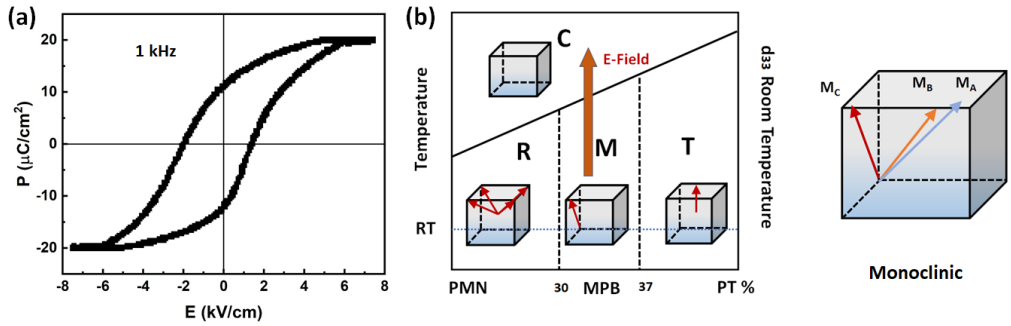

Figure 5.2: (a) P-E loop for PMN-0.3PT, (b) phase diagram of PMN-PT around MPB and illustration of Monoclinic structure.

behavior can be attributed to the generation of an internal bias (E_i) inside the ferroelectric substrate, which is defined as $E_i = (E_c^+ - E_c^-)/2$. This internal bias is caused by the pinning effect by domain walls in which the spontaneous polarization is absent or suppressed resulting in an asymmetric hysteresis loop[30]. For instance, it can be noted that the interface regions between the substrate and the electrodes act as a location of space charge accumulation, which could represent another source of internal bias field responsible for deformations and asymmetries in hysteresis loops[101]. Also, PMN-PT single crystal near MPB composition exhibit a local phase transition or co-existence of different phases not only with changing temperature but also by applying electric field [102]. This MPB region exists from approximately 0.3–0.37 mole fraction of PT, in which the piezoelectric properties have the highest response [103]. Recently, the behavior of this MPB region has been understood concerning the easy rotation of the polarization direction through the formation of intermediate stable monoclinic structures [104]. Figure 5.2(b) represents the temperature - PT composition phase diagram around MPB region, and the polarization directions of the intermediate monoclinic structure (MA, MB, and MC). These complex structures give rise to the formation of additional internal bias by application of E-field. By calculating the internal bias generated by E-field on the FE substrate during measurements, it showed a value of about 1 kV/cm.

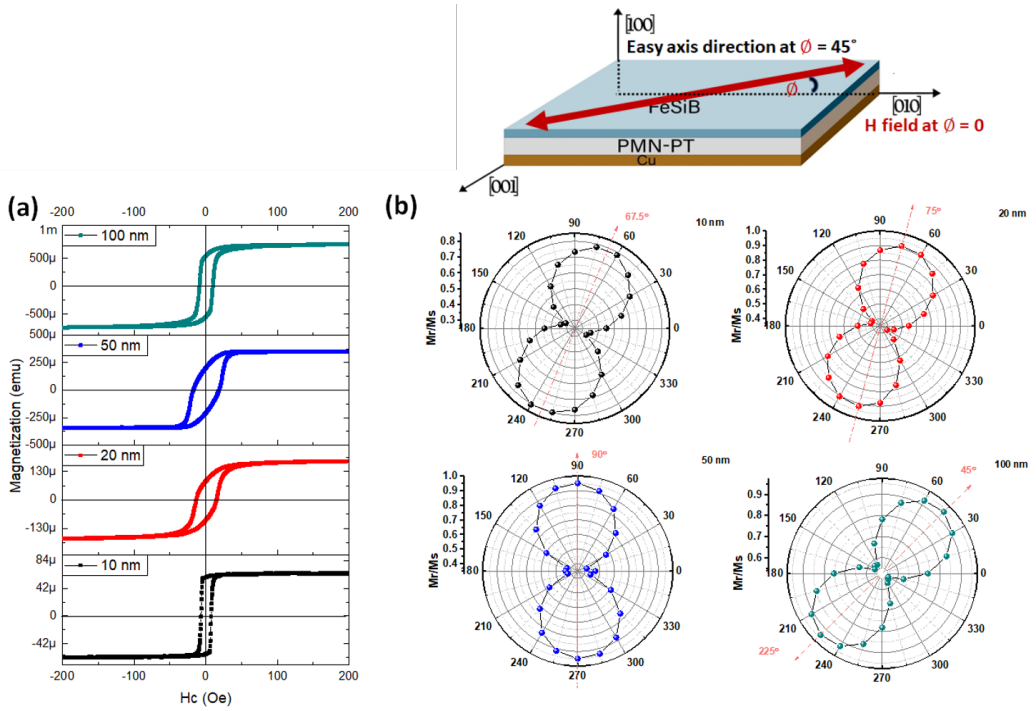

Figure 5.3: (a) M-H loops for the as deposited FeSiB films with different thicknesses, (b) Angle dependent of normalized M_r for all studied thicknesses.

5.3.2 Magnetic properties

For magnetic measurements, in-plane hysteresis loops of M-H curves for different thicknesses were measured by the application of magnetic field along [010] direction (parallel to the structure). The studied FeSiB thin films result to be strongly affected by the film thickness. As shown in Fig. 5.3 (a) M-H curve for 10 nm showed a soft magnetic property with low coercivity H_c = 10 Oe. By increasing thickness, the coercivity increases and then decreases at 100 nm. From the literature, the origins of the coercive force are imperfections and magnetocrystalline anisotropy that give rise to the hysteresis of magnetic materials [105]. For further understanding of the thickness-dependent of magnetic properties, in-plane angle dependence of normalized M_r was measured for all thicknesses. Φ is the angle between the directions of the applied magnetic field (H) and the easy axis. Figure 5.3 (b) shows a uniaxial anisotropy with an easy axis of 67.5° for 10 nm and by increasing the thickness the direction of the uniaxial anisotropy rotates to

be at 75°, 90°, and $45/255^{\circ}$ for 20,50 and 100 nm, respectively. The appearing uniaxial anisotropy is mainly induced due to the stress applied to the films during sputtering indicating the change in the anisotropy[106, 107]. By increasing the film thickness, the anisotropy easy axis rotates due to different strains introduced to the FM films. These strains are generated from the induced interface defects and the anisotropy from the magnetic field induced during sputtering (produced nanograin crystalline structure in the amorphous matrix), also PMN-PT substrate introduces strains to the deposited FM films. We can say that the anisotropy direction from deposition is equal for all thicknesses while the contribution of the interfacial anisotropy reduced at higher thicknesses and the effect of PMN-PT strain increased due to the increase of the deposition time. The difference in the interaction between different sources of the uniaxial anisotropy with different thicknesses makes the uniaxial anisotropy easy axis to rotate. We can conclude that the effective anisotropy energy at different thicknesses is described as the following relation.

$\mathrm{K}_{(}eff) = \mathrm{K}_{(}naocyrtallites) + \mathrm{K}_{(}interface) + \mathrm{K}_{(}substrate)$

Figure 5.4 shows the thickness-dependence of coercive field and normalized Mr at [010] direction. This figure indicates the dependence of the coercive field on the anisotropy direction of the different film thicknesses at the virgin state (before E field application). As we described the magnetoelastic energy (due to strain coming from deposition) is constant in the film plane. Therefore, the cause for anisotropy changes is owing to the induced interfacial defects in FeSiB/PMN-PT interface and PMN-PT Piezo-strains.

5.3.3 Static magnetoelectric properties

To investigate the electric field tuning of magnetic properties of our studied structure, static ME coupling of multiferroic heterostructures of 10, 20, 50, and 100 nm FeSiB/PMN-0.3PT was studied by electric-field induced changes in M-H hysteresis loops. The electric field was applied across the structure thickness as shown in Fig.

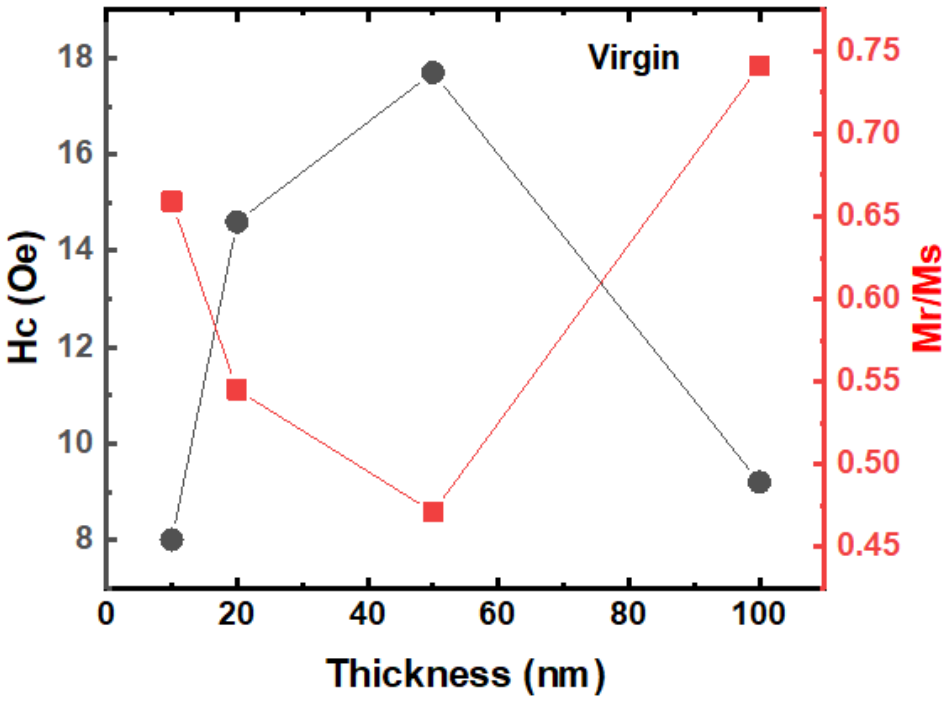

Figure 5.4: H_c and M_r as a function of film thickness at virgin state.

5.5, and magnetization hysteresis loops are measured in-plane under different values of bipolar applied electric field E. Generally, the obtained converse ME coupling effects are all dependent on interfacial effects, i.e., interfacial strain propagation and interfacial charge accumulation[40, 108]. Figure 5.6 (a) represents the measured M-H loops for 10 nm thick of FeSiB under the application of bipolar E field as a representative for thinner films. From the figure, we can see that there is a linear and systematic increase in the coercivity (H_c), and a decrease in remnant magnetization (M_r) of the ferromagnetic film by increasing the applied electric field at the negative direction (E-field pointing to the FM film). The E field induces a maximum increase in coercivity by 65 % and a decrease in remnant magnetization by 14 % for 10 and 20 nm thick films. However, by application of electric field in the opposite direction (pointing away from the film), there is an abrupt increase in coercivity at 2 kV/cm, showing a distorted loop shape and asymmetric behavior for both 10 and 20 nm thickness. We confirmed

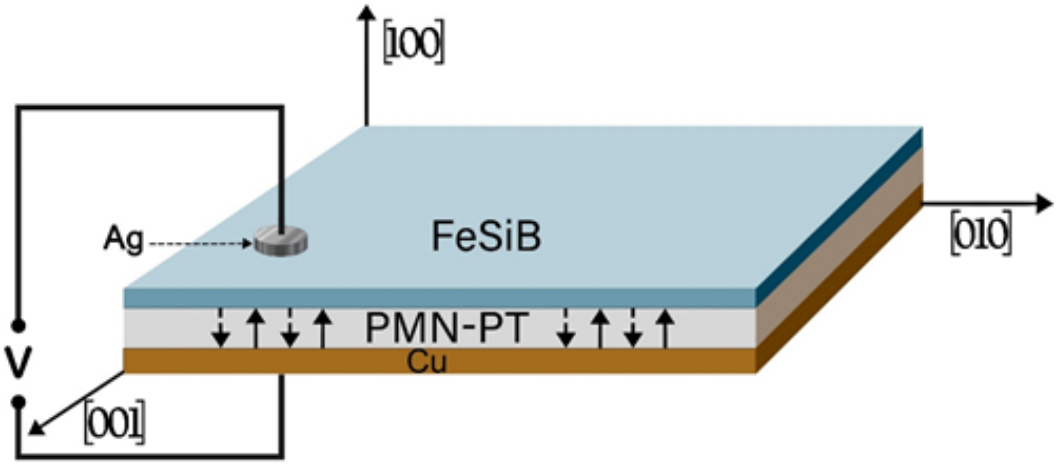

Figure 5.5: Schematic illustration of FeSiB/PMN-PT under E field application.

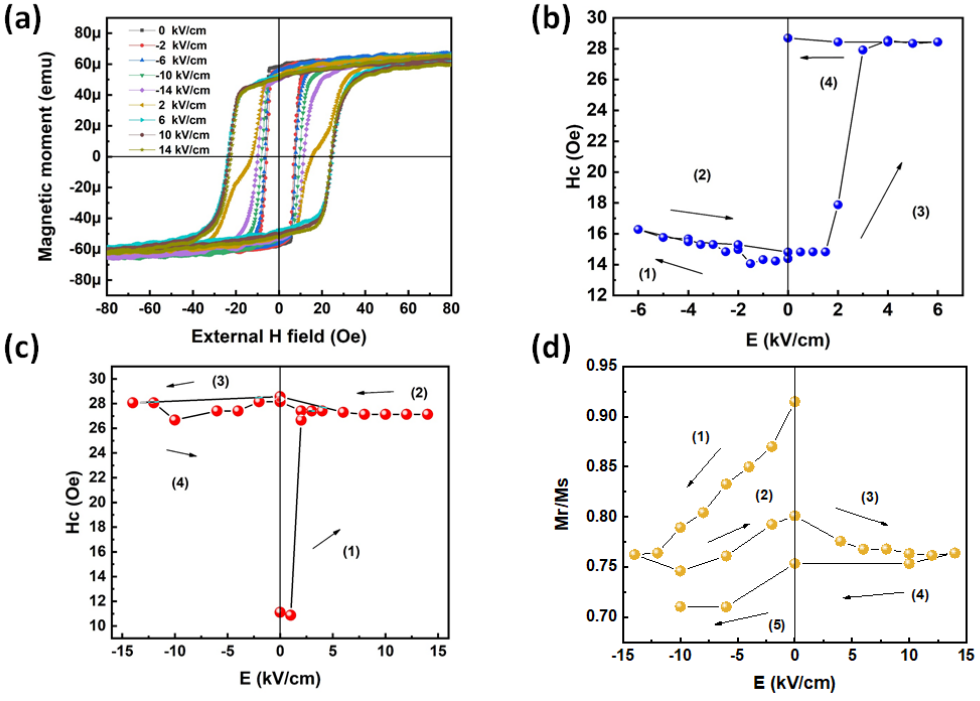

Figure 5.6: (a) M-H loops for 10 nm FeSiB under application of bipolar E field. (b) and (c) are the measured H_c at bipolar E field started from negative/positive field,respectively. (d) M_r as a function of bipolar E field.

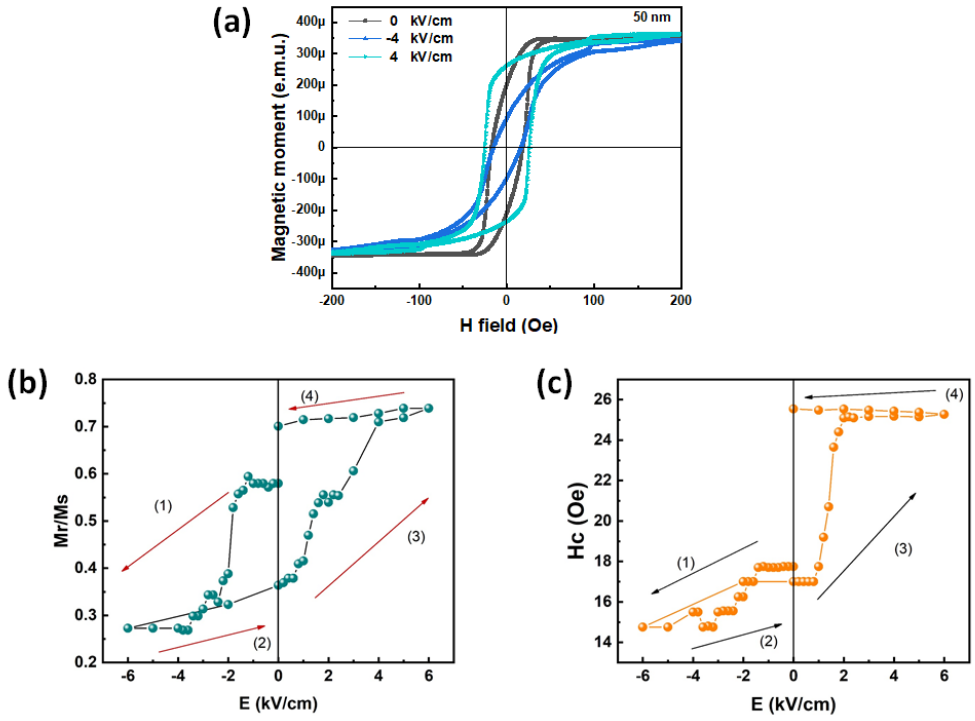

Figure 5.7: (a) M-H loops for 50 nm FeSiB under application of bipolar E field. (b) M_r as a function of bipolar E field and (c) the measured H_c at bipolar E field.

this asymmetric behavior which depends mainly on the sign of the applied E field by sweeping the E field from positive to negative direction as shown in Fig.5.6 (b) and (c). Furthermore, with applying E-field up to 6 kV/cm the increase in coercivity reaches its highest percentage by 290 %, while the decrease in magnetization reaches 18.5 % as shown in Fig. 5.6 (d). This behavior of E field modulation of the magnetic properties was confirmed for the small thicknesses (10 and 20 nm thick) which strongly indicates the charge effect at the interface plays an important role in magnetoelectric coupling for the small thicknesses as we will discuss later.

On the other hand, there is a major change in the magnetic anisotropy observed by increasing film thicknesses up to 50 and 100 nm. Figure 5.7(a) represents the M-H loops under E field application of 50 nm thick of FeSiB as a representative of large thickness. There is significant modulation of the magnetic anisotropy under the application of bipolar E field across the film thickness. We can realize this change by measuring the E field dependence of M_r and H_c as shown in Fig.5.7 (b) and (c). There is a gradual decrease in both M_r and H_c by increasing negative E field, while there is a gradual increase in M_r and H_c by increasing positive E field. This observed behavior is strongly related to the strain effect which transferred from PMN-PT substrate through the combined piezoelectric and magnetoelastic properties of both FM and FE layer[108]. This behavior is also confirmed for the highest thickness 100 nm FeSiB. We can say that the application of negative E field introduces compressive strains, while the application of positive field introduces tensile strains to the PMN-PT substrate which is transferred to the FM layer.

5.3.4 Voltage driven Angle dependent changes in Hc and anisotropy

Figure 5.8 shows the angular dependence of normalized remanence magnetization (Mr/Ms) curves under electric fields of 0 kV/cm (unpoled state) for all studied film thicknesses, while Fig. 5.9 represents the angular dependence of H_c. As shown in Fig. 5.8, for the small thickness 10 and 20 nm there is a slight change in the anisotropy

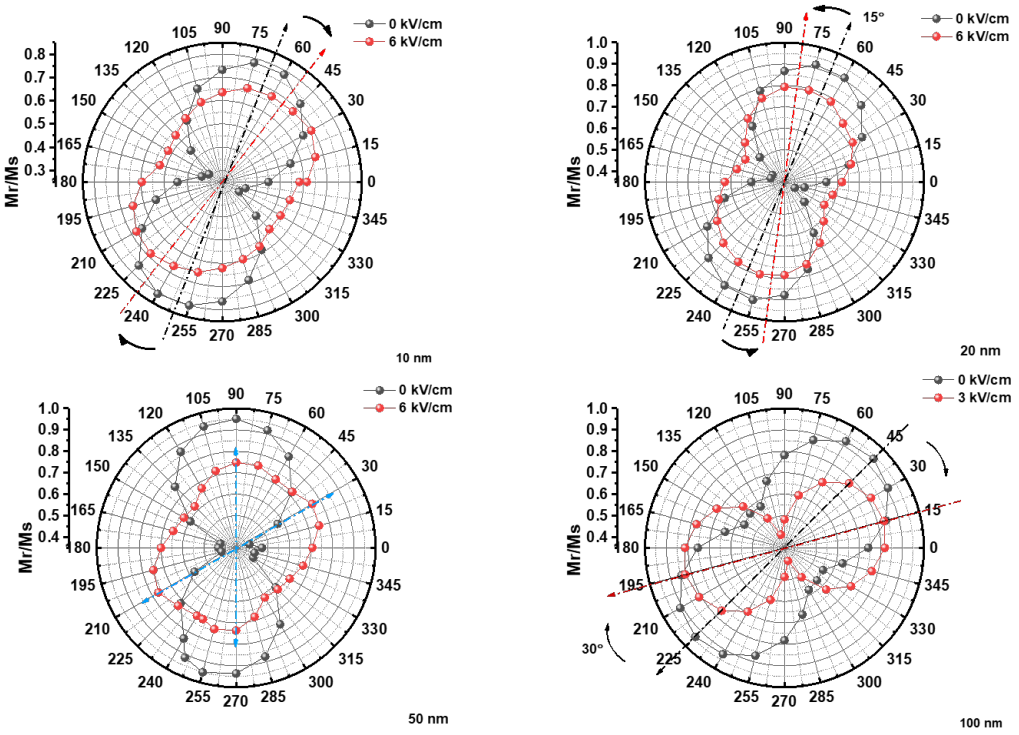

Figure 5.8: Angle dependence of normalized M_r before and after E field application for all studied FeSiB thicknesses

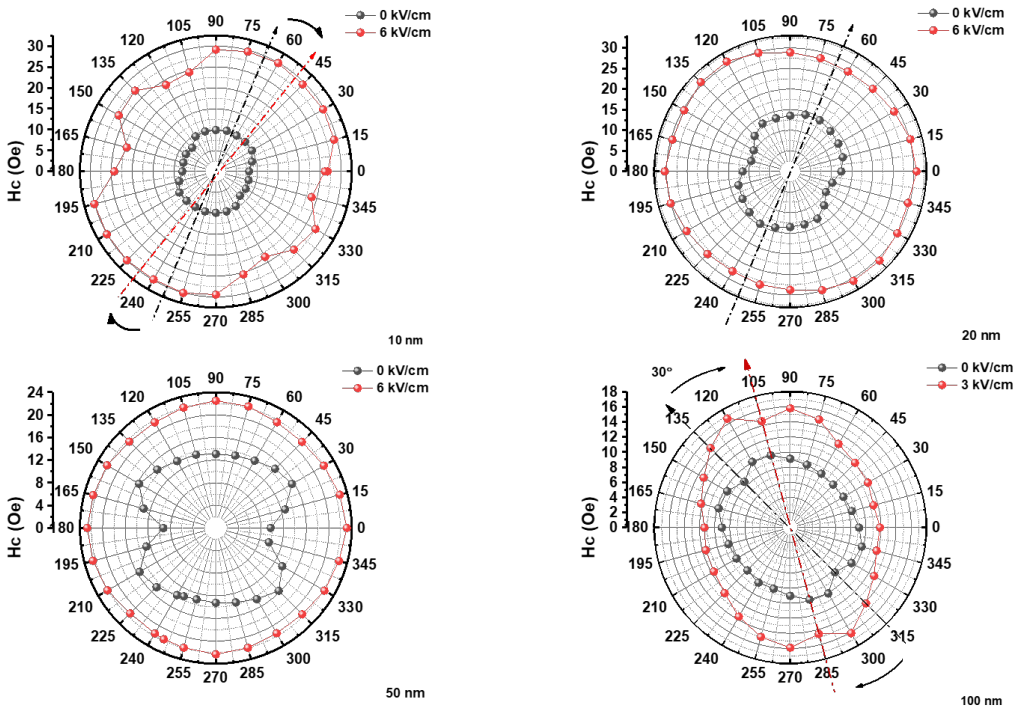

Figure 5.9: Angle dependent of normalized H_c before and after E field application for all studied FeSiB thicknesses

easy axis direction by 15 ° at E field of 6 kV/cm. While the main change appears for Hc which is changed to a four-fold state and increased significantly in magnitude by applying E-field. For thicker FeSiB film with thicknesses of 50 and 100 nm, by applying an electric field of 6 kV/cm the two-fold symmetry seems to disappear and a four-fold symmetry appears for the film thickness 50 nm, which can be explained as the electric field induces a four-fold cubic magnetocrystalline anisotropy to the FeSiB layer due to the strained state on the interface layer. However, for 100 nm thickness, there was a 30° change in the anisotropy easy axis direction. While the Hc shows four-fold transition by applying E-field for both thicknesses. Also, by removing high electric poling of 6 kV/cm the film anisotropy and Hc show non-volatile behavior stimulated by the application of high E-field. This change in the FM film properties can be understood by both stain and charge co-medieted ME coupling.

5.3.5 Mechanisms of E field control of magnetic properties

We can say that the voltage-induced magnetic anisotropy and coercivity changes come mainly from two contributions, i.e., magnetoelastic contribution modified via piezo-strain of the PMN-PT and the interface charges contribution modified via spin polarized charges induced by the electric field application.

(1) Strain effect: We can understand the piezo-strain effect of the PMN-PT substrate by its unique ferroelectric domain structure as shown in Fig.5.10. The unpoled state represents the PMN-PT state with the Rhombohedral structure before E field application in which the dipoles have the possibility to be oriented at the eight corners of the cubic cell (8R state) as shown in Fig.5.10 (a). When the E field is applied across PMN-PT thickness, the electric dipoles start to align at the <111> direction of the unit cell (4R state) as shown in Fig5.10 (b). By reversing the E field direction, the polarization starts to switch by the three different domain wall movements 72°, 180 ° and 109 °. The 72° and 180 ° switch at the in-plane direction, while the 109 ° have a 90° switching. We can emphasize that the huge and non-volatile piezoelectric effect

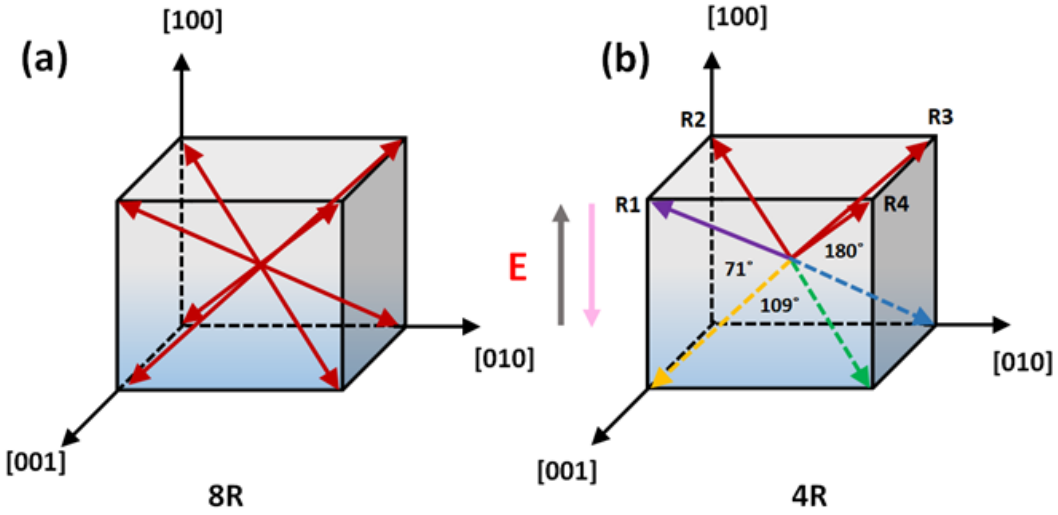

Figure 5.10: Illustration of the polarization switching of the rhombohedral PMN-PT.

of the PMN-PT substrate is induced by the 109 ° domain wall switching[109, 110]. These strains are transferred to the FM layer through the magnetostriction properties of FeSiB film and then changes the magnetic anisotropy.

(2) Charge effect: In order to understand the magnetoelectric mechanisms which contribute to magnetization changes by E field, we studied the interface region of 10 nm FeSiB/PMN-PT heterostructure before and after E field application. X-ray photoemission spectroscopy (XPS) provides a clear understanding of the interface chemistry and bonding so we used XPS as a tool to examine the interface layer between the FM and FE phases[111]. As shown in Fig.5.11 (a), XPS spectra for all contributed elements show the existence of intermediate mixed layer induced due to high sputtering energy represented by Fig. 5.11 (b). XPS spectra of Fe and lead shows their diffusion beyond the interface layer as shown in Fig.5.11 (b) leading to the presence of a mixed interface layer between FeSiB and PMN-PT. Figure 5.12 represents the fitted XPS spectra at the interface region. From O1s spectra, we have confirmed the existence of oxygen vacancies peak (VO) at a binding energy of 531 eV beside the lattice oxygen peak (LO) which has the energy of 529 eV at the interface region as shown in Fig. 5.12 (a). We have also confirmed the existence of FeO peak at 708.4 eV from Fe2p spectra as shown

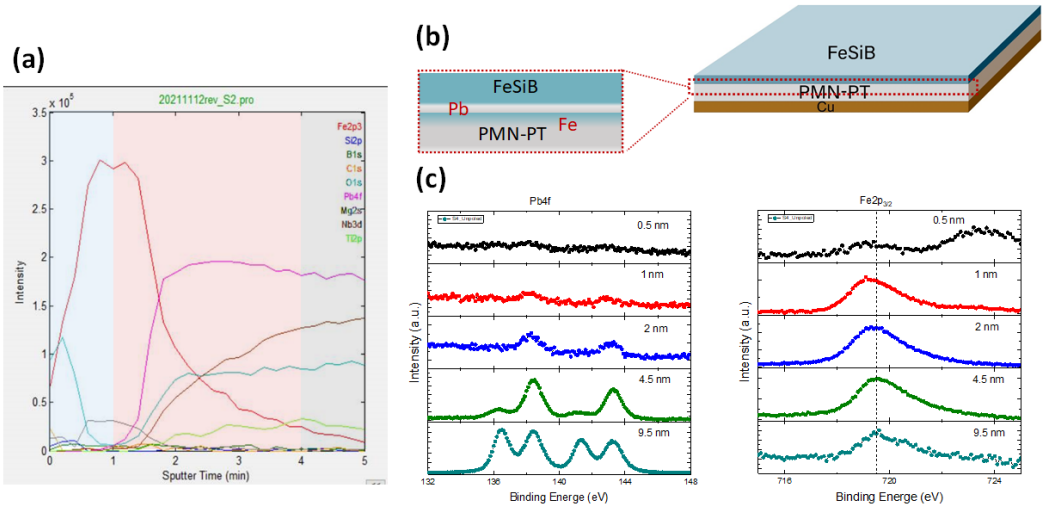

Figure 5.11: (a) XPS spectra at the interface region for all elements, (b) illustration of the mixed interface layer. (c) XPS spectra for Fe and Pb ions during milling.

in Fig. 5.12 (b). The presence of the oxygen vacancies and FeO at the interface layer is mainly induced due to high sputtering energy during deposition. We can say that due to the oxygen vacancies at the interface, the ferroelectric polarization act as an E-field at the interface (field effect) which can tune the local charge densities (electron-hole). The accumulation/depletion of the charge at the interface layer can also affect the orbital occupancy of the magnetic layer resulting in modulation of the magnetic moment which can be noticed from the shift of Fe and Pb spectra under E field application as shown in Fig.5.13. E-field-driven charge carrier movement is polarity dependent and results in strong permanent (nonvolatile) changes. This accumulation/depletion of the charge at the interface layer act as pinning sites which will hinder the domain wall motion of the ferromagnetic layer resulting in a large and non-volatile increase in the magnetic coercivity H_c shown at the small film thicknesses[112]. From our results, we find that the magnetic anisotropy energy density decreases with the increase of electric fields. This confirms that the origin of the electric-field effect on the anisotropy is related to the modulation of interfacial magnetic anisotropy, which is governed by the accumulation/depletion of spin polarized charges. Also, E field is more likely to induce the increase of domain walls due to inhomogeneities of the magnetizing phases

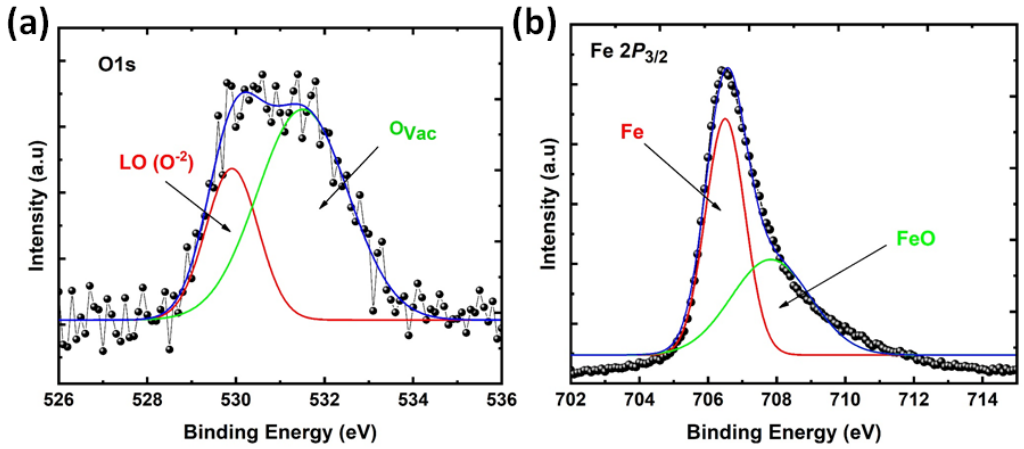

Figure 5.12: (a) XPS spectra for O1s, (b) XPS spectra for Fe2p.

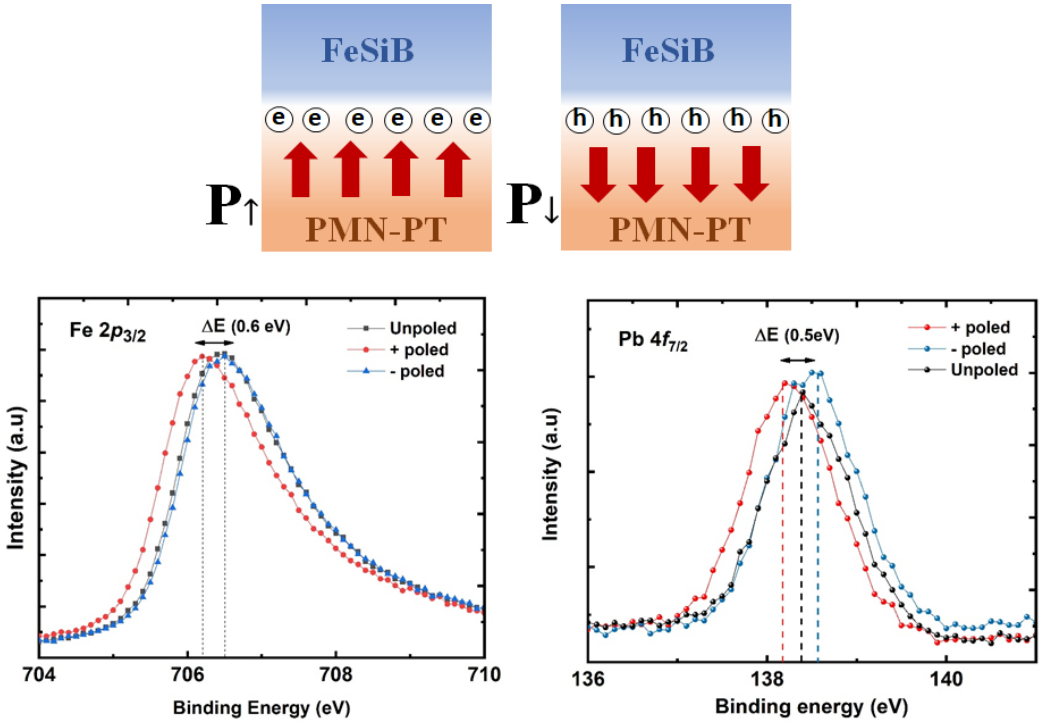

Figure 5.13: XPS spectra for Fe and Pb ions under the application of E field and the illustration of the charge accumulation/depletion.

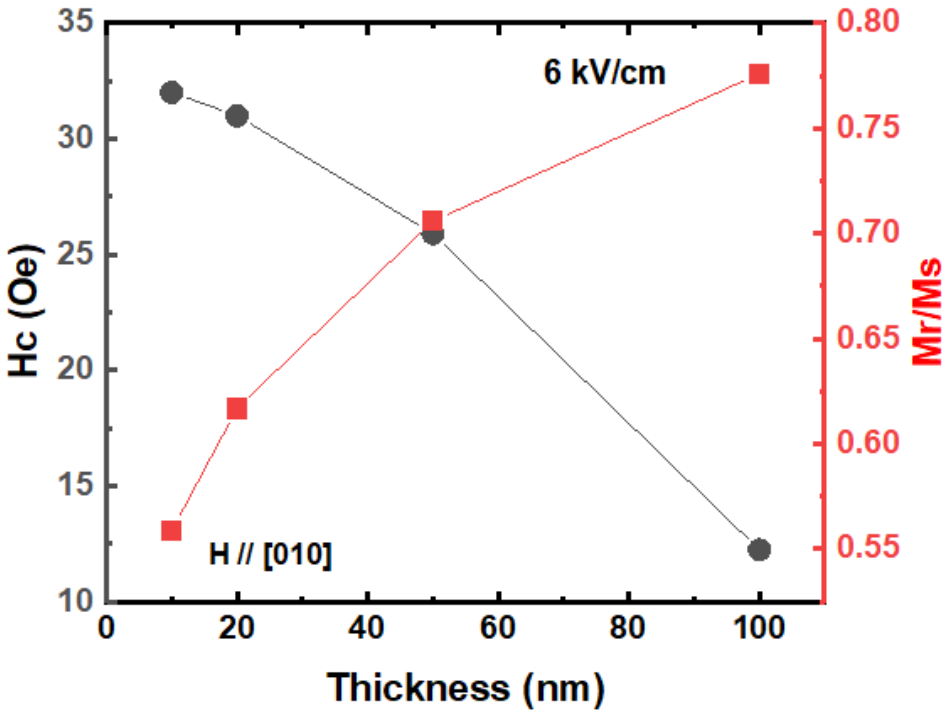

Figure 5.14: H_c and normalized M_r at E field of 6 kV/cm as a function of film thickness

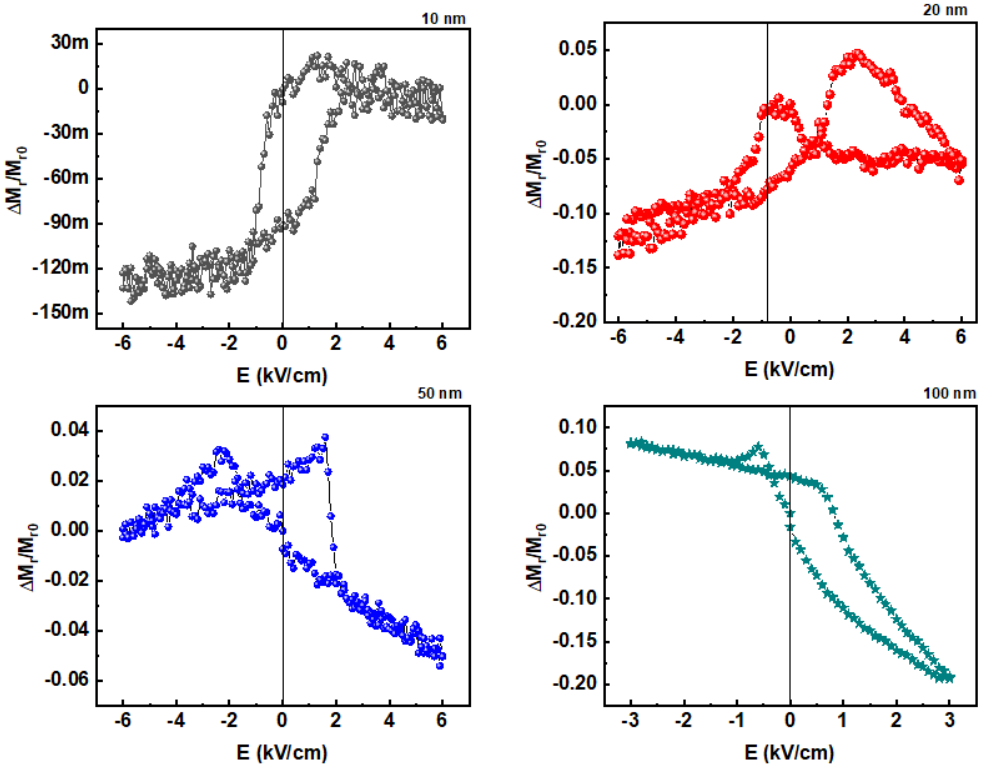

Figure 5.15: M_r-E loops for all studied film thicknesses.

at the interface (the charge accumulation is spin polarized and contributes to the total magnetization at the interface) which is the origin of the higher coercive field for the smaller thicknesses. E-field control of coercivity (H_c) shows a thickness-dependent behavior as shown in Fig. 5.14. By applying an E field of 6 kV/cm, FeSiB film shows lower coercivity and higher magnetization by increasing film thickness which indicates the interface charge effect is dominant at smaller thicknesses. At smaller thickness, the effect of the interfacial spin polarized charges will hinder the magnetization reversal due to pining of domain wall and hence increase the Hc. As the thickness increases, the interfacial effect decreases and the most dominant effect is the strain which increases the in-plane anisotropy due to the spin-dipole interaction.

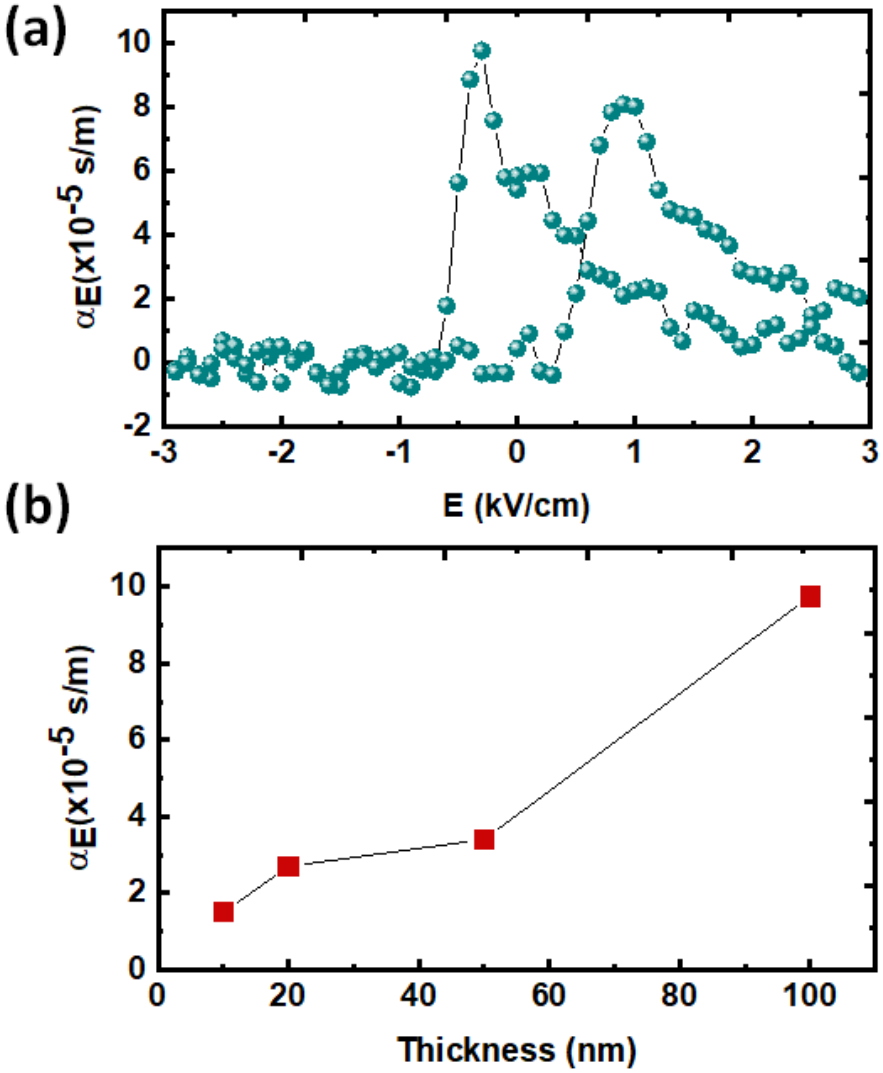

Figure 5.16: (a) derivative M_r-E loops. (b) CME constants as a function of film thickness.

5.3.6 M-E measurements

In order to estimate the convert magnetoelectric coupling for our multiferroic heterostructure, we studied the dependence of the remnant magnetization, M_r, on E field. Figure 5.15 shows the dependence of the remnant magnetization, Mr, on electric field (Mr–E curves) for the in-plane [010] direction for all studied thicknesses. The results show a square-shaped M–E loop which confirms the interfacial cooperation of strain and charge effect for 10 nm. By increasing thickness, the loop changes to mixing of hysteresis and butterfly shape, until it shows a fully asymmetric butterfly shape with the thickness of 100 nm. The hysteresis-shaped M–E loop confirms the interfacial charge effect, which is different from the asymmetric butterfly-shaped induced by the stain of PMN-PT substrate. We also calculated the magnetoelectric coupling coefficient by differentiating M_r with E field according to this equation as shown in Fig. 5.16 (a).

$$\alpha_{CME} = \mu_0(\Delta M_r/\Delta E) \tag{5.1}$$

Figure 5.16 (b) shows the magnetoelectric coupling calculated for all film thickness. The CME constant shows very high values which increase by increasing the film thickness and ranging from 1.5 10^{-5} to 9.75 10^{-5} s/m. This increase of CME constant indicates the dominated strain effect related to the ferroelectic domain wall switching in PMN-PT substrate which is the main driven ME force at larger thicknesses.

5.3.7 Microwave Magnetoelectric Interaction

FMR absorption is an interesting resonance phenomenon that occurs when a magnetic field and a microwave field are applied to a ferromagnetic sample at the same time, and the resonance condition is obtained[77]. A large number of research achievements have been reported on E field tuning of FMR involving a wide range of geometries and materials[113]. E field control of magnetism may introduce a wide FMR modification in an energy efficient way for spintronic devices applications[114]. Figure 5.17 (b)

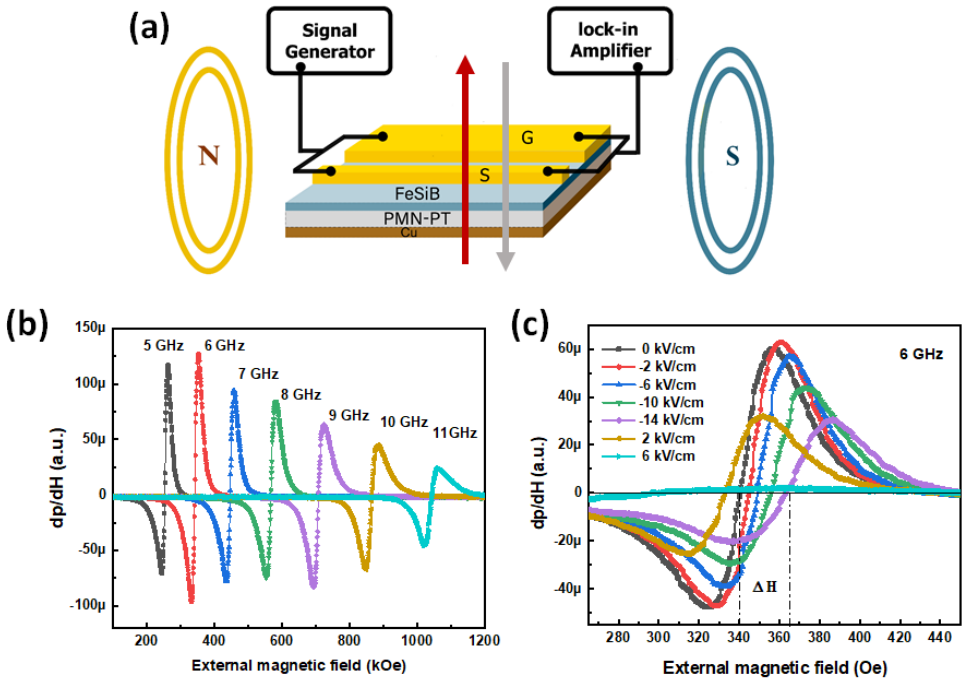

Figure 5.17: (a) Schematic illustration of FMR measurements. (b) FMR spectra at different frequencies. (c) FMR spectra at 6 GHz under the application of bipolar E field.

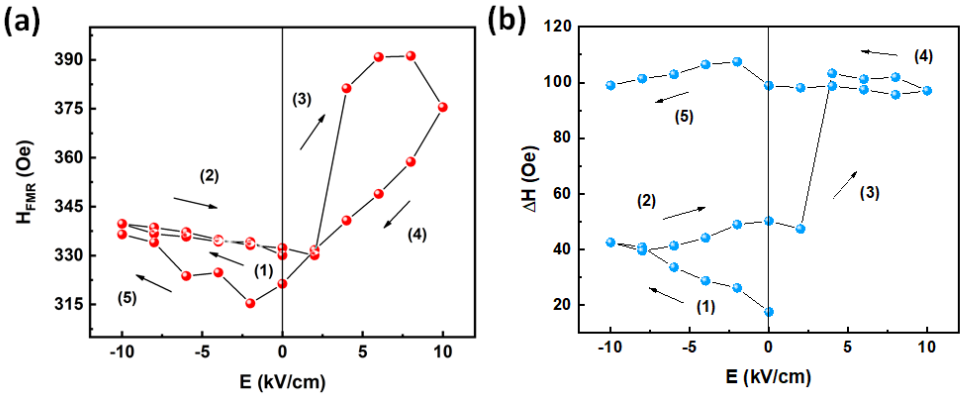

Figure 5.18: (a) E field dependent of FMR resonance field. (b) E field dependent of FMR linewidth.

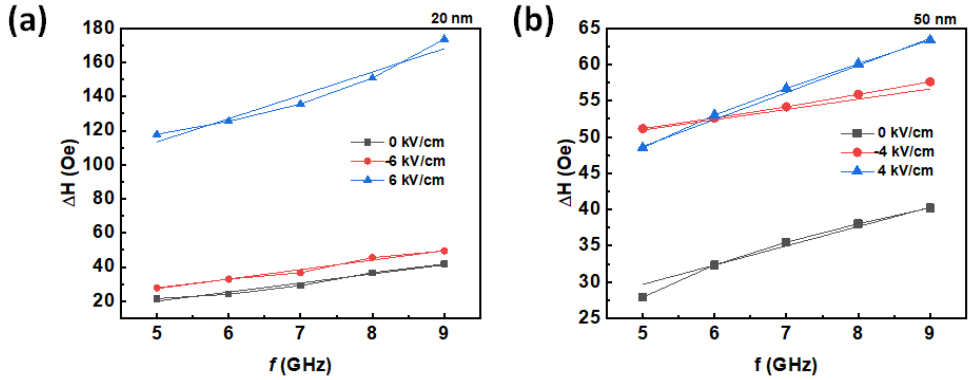

Figure 5.19: (a) and (b) represents FMR linewidth as a function of frequency at bipolar E field for 20 nm and 50 nm, respectively.

shows the FMR spectra of 10 nm FeSiB as a representative thickness to investigate the microwave ME interactions with the magnetic field along to [010] direction of PMN-0.3PT substrate. The E field is applied across the structure thickness as shown in Fig. 5.17 (a). Room temperature fixed frequency (from 5 GHz – 11 GHz) FMR measurements were performed in field sweep mode using Cu-coplanar waveguide in flip-chip geometry. Figure 5.17 (b) shows the FMR spectra for our studied heterostructures, which indicates the resonance field and corresponding linewidth at each corresponding frequency. We have observed that the frequency of 6 GHz has the highest absorption among all frequencies for all studied thicknesses.

To investigate the effect of the electric field on microwave magnetoelectric interaction, the dynamic magnetoelectric response of the films was investigated at a frequency of 6 GHz under different bipolar electric fields as shown in Fig.5.17 (c). We swept the electric field from negative to positive (similar to the static measurements). As shown in the figure, a gradual shift up to 24 Oe in the resonance field is induced by increasing the field to -14 kV/cm and shift by 75 (Oe) at 14 kV/cm, showing asymmetric behavior. We can understand the E field tuning of FMR spectra as follows. The electric field induces a deformation of the ferroelectric substrate resulting from the 109° ferroelectric domain wall motion which introduces strains. This stained state transmitted to the magnetic FeSiB film via the convert magnetoelectric (CME) coupling. Usually, the

change in FMR field is due to spin-orbital coupling and the magnetostriction induced by the strain from PMN-PT. However, the change exhibits asymmetric behavior between the positive and negative E fields which can be attributed to the cooperation of the interfacial strain and charge mediated coupling.

Figure 5.18 (a) and (b) shows the FMR resonance field (H_{FMR}) and the peak-to-peak FMR linewidth (ΔH) as a function of applied electric field which are extracted from the FMR spectra that fitted to the derivative of a modified Lorentzian function[115]. The H_{FMR} field and ΔH exhibit a strong dependence on the electric field showing a gradual increase by increasing the electric field. This simultaneous modification of ΔH and H_{FMR} is attributed to the strain in the magnetostrictive FeSiB film. As shown in the figure that at E = 6 kV/cm there is a dramatic change in the FMR field and ΔH supporting the results obtained from static measurements. The asymmetric increase in FMR linewidth with E-field may indicate the two-magnon scattering due to the charge effect. Also, the E-field modulation of FMR resonance shows mixed loop/butterfly shape which indicates the cooperation of stain and charge effect. We can assume that the main mechanism responsible for the asymmetric phenomenon is related to the accumulation/depletion of the spin polarized interfacial charges. This interfacial charge restricts domain wall movement and generates biased polarization and additional strain states at the interface layer. Additionally, not only was a shift in the resonance field obtained, but also a decrease in the amplitude of the FMR spectra and broadening of FMR linewidth with increasing electric field was observed, which indicated that the excitation triggered by the electric field was transferred to the spin system via the magnetoelectric coupling.

The FMR linewidth ΔH consists of the intrinsic Gilbert damping contribution (parameterized by the damping constant α) and the frequency-independent inhomogeneous linewidth broadening ΔH_0 [115].

$$\Delta H = \Delta H_0 + (4\pi\alpha)/(3\gamma)f \tag{5.2}$$

where f is the microwave excitation frequency and γ is the gyromagnetic ratio. According to Eq. (5-2), α and ΔH_0 can be determined directly by measuring the frequency dependence of ΔH. Figure 5.19 (a) and (b) represent FMR linewidth (ΔH) as a function of frequency for 20 nm and 50 nm of film thickness, respectively. It has been found that the FMR linewidth increases with frequency at E = 0 kV/cm. By application of an electric field of 6 kV/cm, there is a large enhancement in ΔH values. Also, FMR linewidth becomes increasingly nonlinear with f at higher frequencies for smaller thicknesses as shown in Fig.5.19 (a). Such a nonlinear behavior is related to two-magnon scattering, which comes from coupling between the uniform FMR mode and the degenerate spin waves due to the interfacial spin polarized charges, leading to an additional magnetic relaxation channel. However, for thicker samples, ΔH increases linearly with f over the entire experimental frequency range indicating the decrease of the interface effect as shown in Fig.5.19 (b). In addition, magnetic damping of FeSiB film has been determined from the linear fits to the FMR linewidth data ΔH using the relation, $\alpha = (\gamma/2\pi f)\ \Delta H$. Generally, spin-orbit interactions are the major origins of magnetic damping for FM thin films[81]. Figure 5.20 shows the FeSiB thickness dependence of the damping constant. As shown in the figure the damping constant decreases with increasing the thickness at E field of 0, -6, and 6 kV/cm, indicating the decrease of the interfacial charge effect. We can say that there is a contribution of two different damping mechanisms in thick and thin films. In thinner films, two-magnon scattering due to the interfacial spin charges is significant for the FMR linewidth, while the Gilbert damping dominates the linewidth in thicker films[116]. As the charges at the interface are spin polarized and contribute to the demagnetizing field and may induce PMA and two magnon scattering effect.

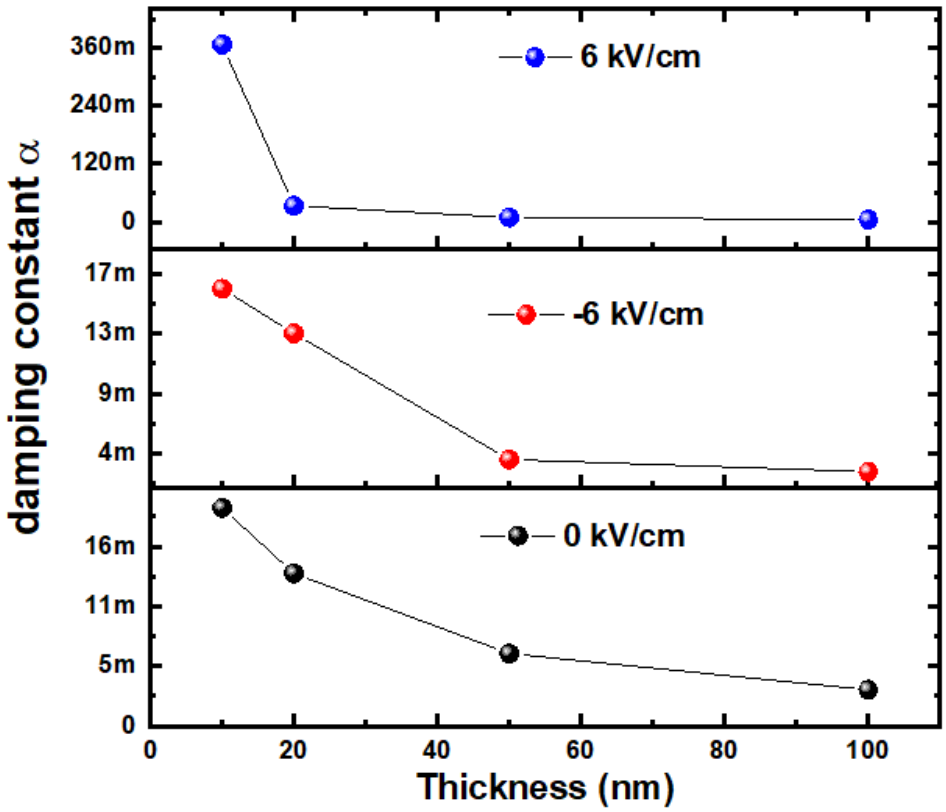

Figure 5.20: Thickness dependent of FMR linewidth at applied bipolar E field.

5.4 Summary

FeSiB films with different thicknesses 10,20,50 and 100 nm was deposited by DC sputtering on top of PMN-0.3PT substrate. The XPS spectra were showed a mixed interface region with the existence of O vacancies and oxidation state of Fe (FeO) at the interface layer between FM and FE layers which was introduced due to the high sputtering energy during the deposition. We have got E-field control of magnetic anisotropy and coercivity Hc depending on E-field polarity and film thickness. We obtained a non-volatile E-field modulation of the static and dynamic magnetic properties through the cooperation of the strain and charge effect, however, the interfacial charge effect is significantly reduced at higher thicknesses and the strain effect dominates. In addition, FeSiB/PMN-PT heterostructures showed very large CME constants ranging from 1.5×10^{-5} to 9.75×10^{-5} s/m for 10 and 100 nm, respectively. We can conclude that our heterostructures show a high potential for memory and energy storage applications.

Chapter 6

E field-modulated magnetism in NiFe/Pt/CoFeB/PMN-0.3PT heterostructure

6.1 Introduction

Electric-field manipulation of magnetic properties in multiferroic is considered an efficient way of authorizing memory and magnetic microwave devices with ultralow power consumption[117]. Multiferroic heterostructure which mainly consists of combined ferromagnetic and ferroelectric layers provides the most consistent and reliable E field tuning of magnetic properties. In this type of heterostructures, strain or charge induced by an electric field applied on the ferroelectric layer is capable of manipulating the magnetic anisotropy of the adjacent magnetic layer, resulting in a magnetoelectric effect[118]. Due to its high piezoelectric coefficient, PMN-0.3PT single crystal with 100 orientation is a good candidate as a FE layer in our study. NiFe film is used in our tri-layer heterostructure due to its high saturation magnetization[119], low coercivity [120] and small ferromagnetic resonance linewidth. Also, CoFeB film is used due to its unique properties like the induced PMA under the application of E field[121]. In

this ME MF tri-layer heterostructures, we aim to study the effect of the E field and the magnetoelectric coupling mechanisms on the interface layers between the two FM films separated by Pt spacer. Usually, at the interface layer between different magnets, there is a possibility of some coupling between the different magnetic layers which leads to modulation of the magnetic properties[122, 123]. By depositing NiFe and CoFeB separated by Pt layer on top of PMN-0.3PT substrate, we aim to control the magnetic properties of the tri-layer by using an external E field.

6.2 Sample fabrication

NiFe, Pt, and CoFeB films of 5 nm thickness of each were deposited on one side-polished unpolarized commercial ferroelectric (100)- oriented single crystal PMN-0.3PT substrates with the dimensions of 5 ×5 ×0.5 mm. The deposition was held by DC sputtering technique at room temperature without an applied external magnetic field. The base pressure of the chamber was kept lower than 2×10^{-5} Pa, and the work power was set to 500 W. During the sputtering process, argon gas was used as the ambient gas at a flow rate of 10 sccm, and a working pressure of 0.2 Pa. For electrical measurements, Cu was evaporated as a lower electrode and Cu wires were connected with silver past to apply E field across the sample thickness.

6.3 Magnetoelectric Static Measurements

Magnetic properties for the tri-layer heterostructure at the virgin state (Before E field application) were measured by M-H loops at 0 and 45 deg, as shown in Fig.6.2. M-H curves show a uniform loop with soft properties and a coercive field of 8 Oe. However the loop at 45 deg shows a higher remnant and lower saturation field indicating the anisotropic property of the deposited films. For further understanding of the magnetic anisotropy of the as-deposited tri-layer, we measured the angle dependence of

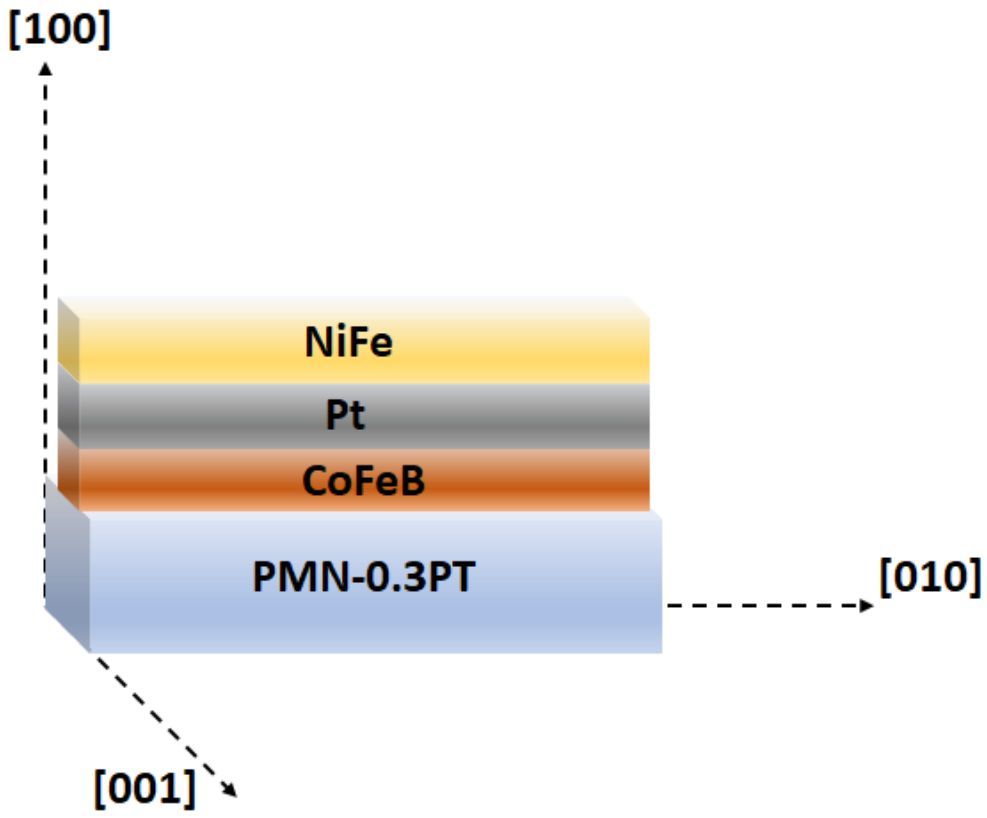

Figure 6.1: Schematic illustration of the Tri-layer heterostructure

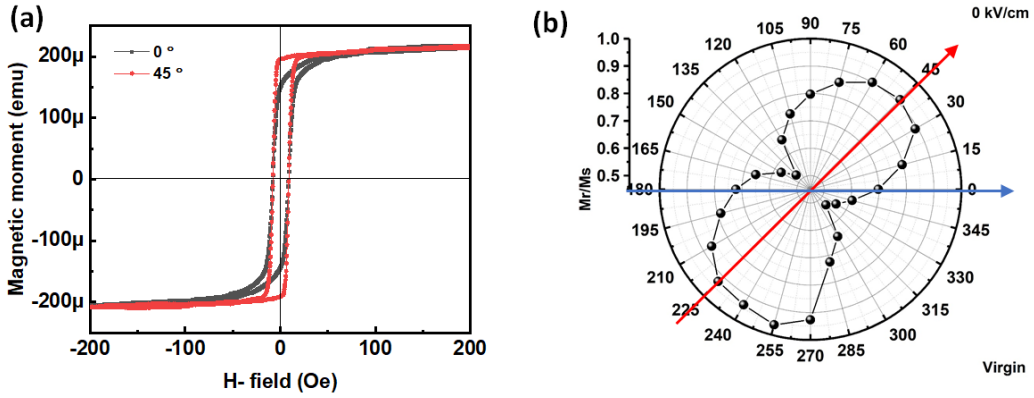

Figure 6.2: (a)M-H loops at 0 and 45 deg, (b) Angle dependent of normalized M_r

normalized M_r. The tri-layer heterostructure shows a uniaxial magnetic anisotropy with an easy axis at 45 deg which is induced during the deposition. From these results, we can see the coupling between the upper and lower magnetic layers. Owing to the unique properties of Platinum it can easily introduce the coupling between CoFeB and NiFe layers which can be understood by the weak ferromagnetism induced in the Pt spacer between two ferromagnetic layers[124]. We can say that the nonmagnetic spacer becomes weak ferromagnet (fm) because of the magnetic proximity effects from two ferromagnetic metals. In this case, the ferromagnetic coupling occurs between two ferromagnetic layers through the exchange coupling via the fM Pt layer[125].

Static magnetic properties under the application of electric field were characterized by M-H loop measurements. Magnetic field was applied parallel to the heterostructure at [010] direction and at the easy axis direction, while E field was applied across the structure thickness. From Fig. 6.3 (a) we can see that, by applying E field at [010] direction we get two-step loops. Also, the increase of the bipolar E field induces an increase of Hc or domain walls and a decrease in magnetization as shown in fig. 6.3 (b) due to the inhomogeneities of the magnetizing phases at the magnetic interfaces. Generally, in strong/weak/strong ferromagnetic tri-layer it can easily tune the magnetic properties by temperature or strains through the change the Curie temperature of the weak magnetic layer[126]. We can say that due to the low curie temperature of Pt

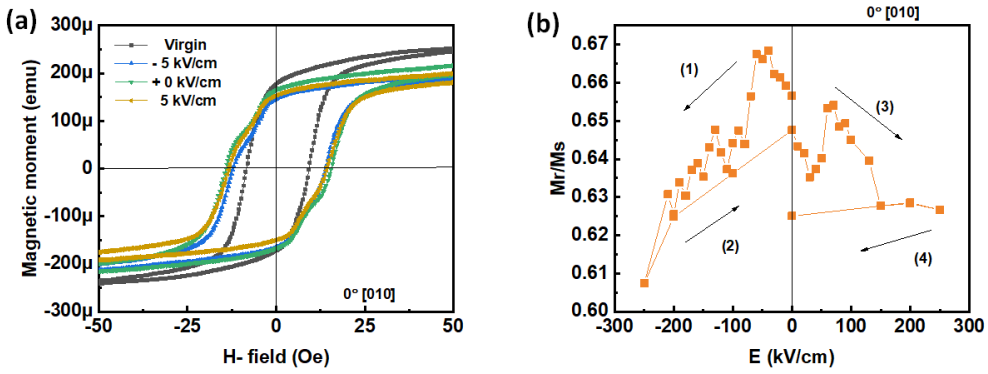

Figure 6.3: (a)M-H loops under the application of bipolar E field at [010] direction, (b) M_r as a function of applied E field.

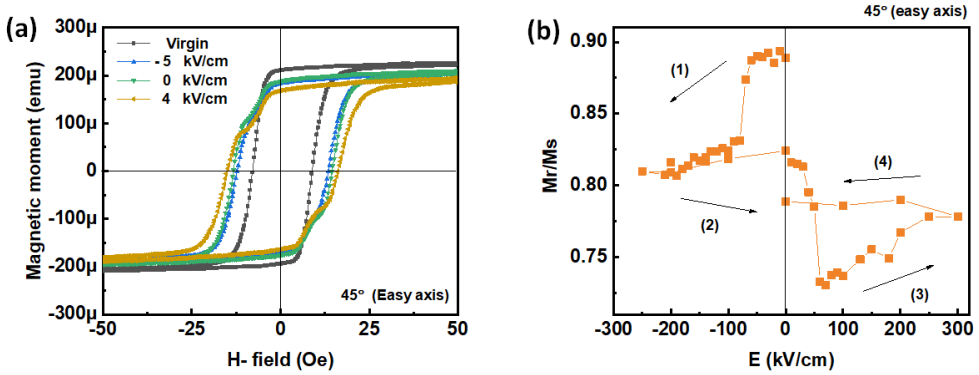

Figure 6.4: (a)M-H loops under the application of bipolar E field at easy axis direction, (b) M_r as a function of applied E field.

which is around room temperature, the E field induces phase transition of Pt layer to become paramagnet and then the two ferromagnetic layers become uncoupled. On the other hand, at the easy axis direction as shown in Fig. 6.4 (a), M-H shows the same properties as shown in [010] direction. However, Fig. 6.4 (b) shows a decrease in M^r by increasing negative E field while it shows an increase by increasing positive E field. we can say that the main mechanism of the E field modulation of the magnetic properties of the tri-layer is that E field introduces some compressive/tensile strains to PMN-PT substrate which depend on E direction through the piezoelectric property. These strains are transferred to magnetic tri-layer and then change the magnetic properties due to magnetostriction property.

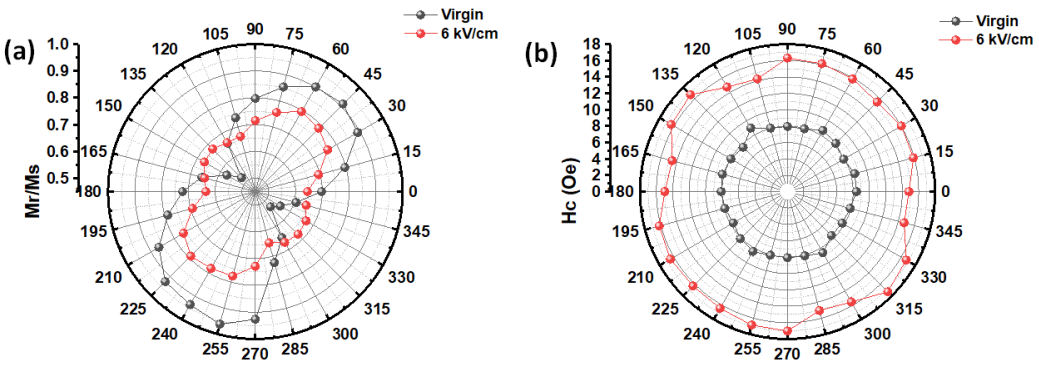

Figure 6.5: (a)Angle dependent of M_r at the virgin state and at 6 kV/cm, (b) Angle dependent of H_c at the virgin state and at 6 kV/cm.

To have a deep understanding of the E field modulation of the magnetic properties of the tri-layer structure we measured the angle-dependent of M_r and H_c before and after the application of E field. As shown in Fig.6.5 (a) at E field of 6kV/cm the uniaxial anisotropy is changed to biaxial anisotropy. Also, H_c shows the same tendency as shown in fig.6.5 (b). we can say that, due to the polarization switching of PMN-PT under the application of electric field, the substrate undergoes a nonvolatile strain resulting from the 109° domain wall switching[109]. These tensile/compressive strains are transferred to the CoFeB layer depending on E field direction and then changes the interfacial anisotropy due to the spin-orbital coupling. This interfacial magnetoelastic anisotropy will affect the interface between magnetic layer making the Pt layer unmagnetized and consequently uncoupling the two magnetic layers.

6.4 Magntoelectric coupling

In order to calculate the magnetoelectric coupling of the tri-layer multiferroic heterostructure, we measured the M_r-E curves. The magnetic field was applied at [010] direction and at the easy axis direction at 200 Oe to reach saturation. After removing the magnetic field, the M_r was measured by sweeping bipolar E field across the structure thickness. Figure 6.6 (a) and (b) show the M_r-E loops at [010] and easy axis

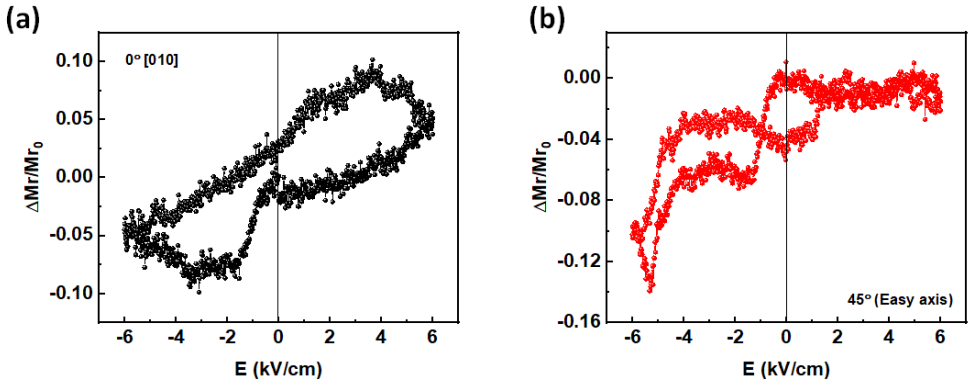

Figure 6.6: (a) M_r-E loop at [010] direction, (b) M_r-E loop at easy axis direction direction.

direction, respectively. From the figure, we can see that the loops have the butterfly shape, which indicates the induced interfacial magnetoelastic anisotropy due to the PMN-PT strain effect. The convert magnetoelectric coupling constant of the tri-layer heterostructure was calculated from M_r-E loop to be 5 to 7.7 x 10^{-5} s/m according to the following equation.

$$\alpha_{CME} = \mu_0(\Delta M_r/\Delta E) \tag{6.1}$$

Such a high value is related to the strain mediated magnetoelectric coupling in the tri-layer heterostructure.

6.5 Magnetoelectric dynamic measurements

Ferromagnetic resonance (FMR) is an important and versatile technique that is widely used for studying magnetic anisotropy and relaxation in thin films and multi-layers[127]. Broadband FMR measurements were performed in field sweep mode using Cu-coplanar waveguide in flip-chip geometry. The magnetic field was applied along [010] direction of the tri-layer heterostructure. As shown in Fig. 6.7 (a) the frequency of 5 GHz has the highest absorption among all frequencies for all film thicknesses. Also, from the figure we can see that the FMR spectra have one uniform absorption peak which indicates

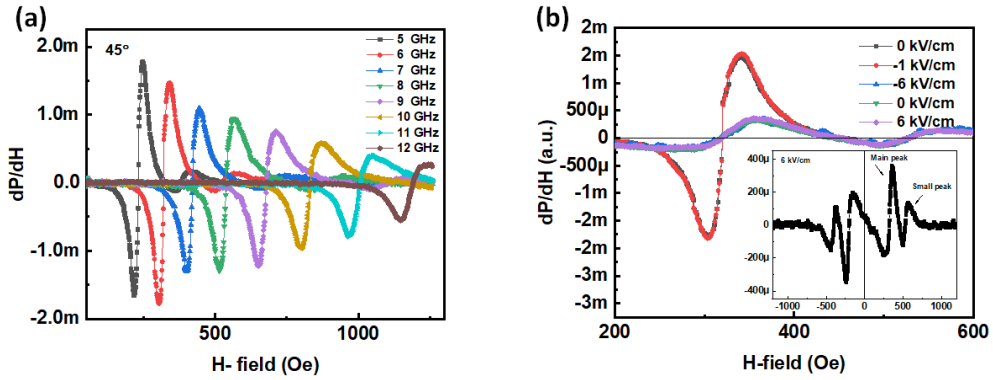

Figure 6.7: (a) FMR spectra at different frequencies, (b) FMR spectra at 6 GHz under the application of E field.

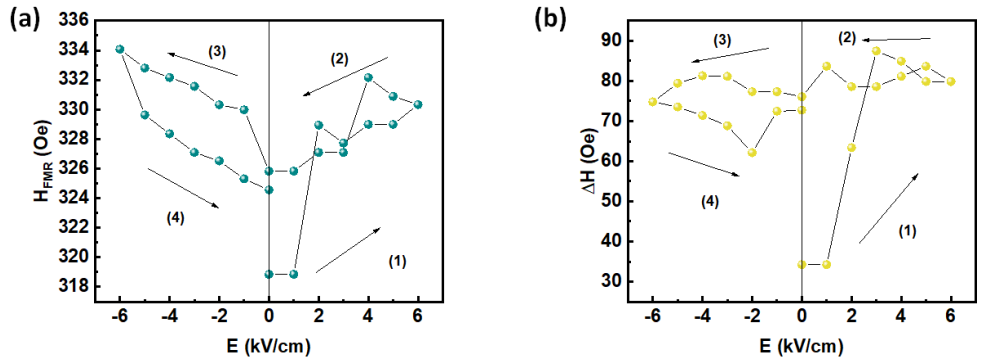

Figure 6.8: (a) FMR spectra at different frequencies, (b) FMR spectra at 6 GHz under the application of E field.

the coupling between the two magnetic layers as confirmed from static measurements.

Because FMR is more sensitive to the magnetization changes, we studied the E field control of the resonance field and damping constant. Figure 6.7 (b) shows the E field modulation of FMR spectra. By applying E field around the saturation field (-/+ 6kV/cm), we obtain a significant modulation of FMR spectra as shown in the inset of fig.6.7 (b). The spectra show a double absorption peak related to the two ferromagnetic layers CoFeB and NiFe confirming the uncoupled state. We can say that the application of the E field introduces interfacial strains at the tri-layer heterostructure. This strain makes the Pt layer unmagnetized and then breaks the coupling between the upper and lower magnetic layers.

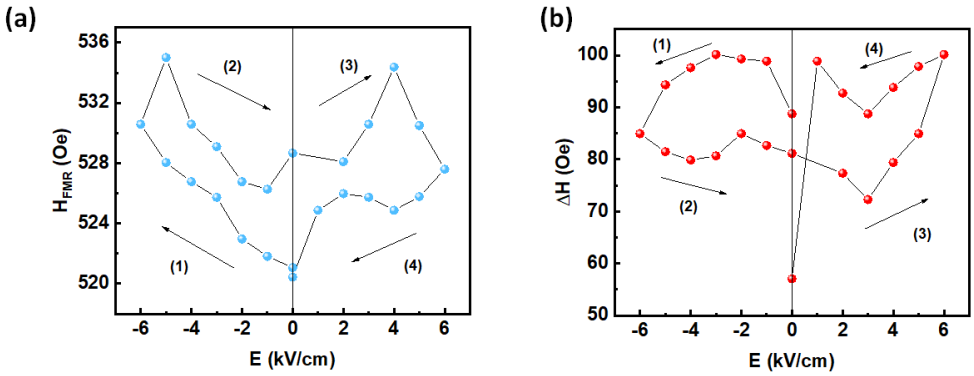

Figure 6.9: (a) FMR spectra at different frequencies, (b) FMR spectra at 6 GHz under the application of E field.

To confirm the strain mediated magnetoelectric coupling of the FMR spectra of the tri-layer and by fitting the FMR spectra, we studied the change of the resonance field H_{FMR} and the FMR linewidth ΔH as a function of the applied E field. Figure 6.8 (a) and (b) shows the H_{FMR} and ΔH changes with E field for the peak related to CoFeB layer, respectively. From the figure, we can see that the loops have the shape of the butterfly which is related to the strain effect from the PMN-PT substrate. The same tendency is shown for the H_{FMR} and ΔH loops related to the NiFe layer as shown in Fig. 6.9 (a) and (b). Figure 6.10 shows the FMR linewidth ΔH as function of frequency. It has been found that the FMR linewidth ΔH shows a linear increase with frequency at E = 0 kV/cm. By the application of electric field of -4 and 4 kV/cm, there is a large enhancement in ΔH.

In addition, magnetic damping of the tri-layer heterostructure has been determined from the linear fits to the FMR linewidth ΔH. Generally, spin-orbit interactions are the major origins of magnetic damping for FM thin films[128]. We can say that by the application of E field the tri-layer structure undergoes compressive/tensile strains which are transferred from PMN-PT substrate. The tri-layer heterostructure shows a damping constant of 0.02141 at E = 0 kV/cm and a value of 0.03308 at E = 4 kV/cm. The large change in α suggests a strong correlation between magnetostriction and the intrinsic Gilbert damping mechanism.

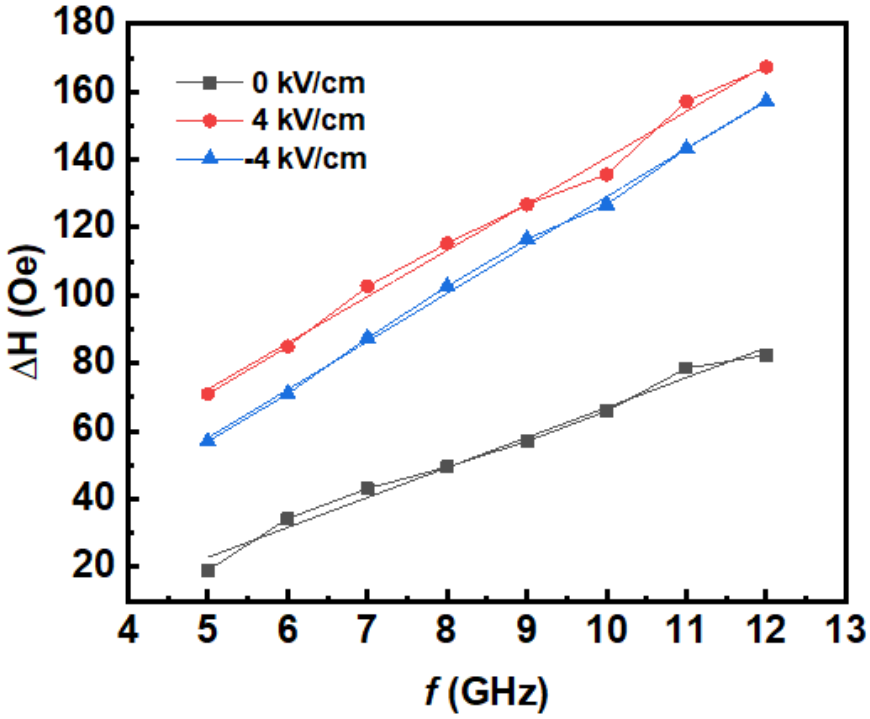

Figure 6.10: (a) FMR spectra at different frequencies, (b) FMR spectra at 6 GHz under the application of E field.

6.6 Summary

NiFe(5 nm)/Pt(5 nm)/CoFeB(5nm)/PMN-0.3PT tri-layer multiferroic heterostructure was fabricated by sputtering technique. We got non-volatile E-field modulation of the static and dynamic magnetic properties through the strain effect related to the 109° polarization switching of ferroelectric domain in (100)-oriented PMN-0.3PT single crystal. The tri-layer multiferroic heterostructure showed a very large CME constant of 7.7 x 10^{-5} s/m related to the strain effect. Also, the damping constant increases by the application of bipolar E field. Due to the strain effect from PMN-PT substrate under the application of E field, the tri-layer system undergoes a change of the interfacial properties. We can say that the Pt layer undergoes a paramagnetic transition which breaks the coupling between the upper and lower magnetic films.

Chapter 7

Conclusion

In this thesis, the main focus was on studying the electric field effect on the magnetic properties of ferromagnetic thin films in newly designed multiferroic heterostructures. To achieve this goal, three different heterostructures were fabricated. By measuring the static and dynamic magnetic properties under the application of bipolar E field, the E field modulation of the magnetic properties was achieved. This convert magnetoelectric coupling is driven mainly by the cooperation of the strain and charge effect at the interface layer of the studied heterostructures. However, the dominant mechanism was the strain effect through the coupling between piezoelectric and magnetoelastic properties of the FM/FE layers.

The detailed conclusion for each experiment is described as follows.

Modulation of magnetic anisotropy in FeSiB film sputtered on curved substrate.

FeSiB film was deposited by sputtering technique on the curved polyimide sheet. Although the conventional soft magnetic property has been confirmed in the FeSiB deposited on the flat polyimide sheet, the systematic change of the magnetic anisotropy was obtained by changing the curvature during the deposition. The significant magnetic anisotropy around 0.15 MJ/m^3 was found to be induced by using the curved sheet with the curvature of 0.15 mm^{-1}. These results indicate that the combination between

the magneto-striction and flexible substrate provides the efficient modulation of the magnetic property.

Thickness-dependent E field-modulated magnetism in FeSiB/PMN-0.3PT heterostructure.

FeSiB film with different thicknesses 10,20,50 and 100 nm was deposited by DC sputtering on top of PMN-0.3PT substrate. The XPS spectra showed a mixed interface region with the existence of O vacancies and oxidation state of Fe (FeO) at the interface layer between FM and FE layers which was introduced due to the high sputtering energy during the deposition. E-field control of magnetic anisotropy and coercivity Hc was found to be depending on E-field polarity and film thickness. A non-volatile E-field modulation of the static and dynamic magnetic properties were achieved through the cooperation of the strain and charge effect. However, the interfacial charge effect was significantly reduced at higher thicknesses and the strain effect dominates. In addition, FeSiB/PMN-PT heterostructures showed very large CME constants ranging from 1.5×10^{-5} to 9.75×10^{-5} s/m for 10 and 100 nm respectively. I can conclude that this multiferroic heterostructure shows a high potential for memory and energy storage applications.

E field-modulated magnetism in NiFe/Pt/CoFeB/PMN-0.3PT heterostructure.

NiFe(5 nm)/Pt(5 nm)/CoFeB(5nm)/PMN-0.3PT tri-layer multiferroic heterostructure was fabricated by sputtering technique. Non-volatile E-field modulation of the static and dynamic magnetic properties was obtained through the strain effect. This strain effect is related to the 109° polarization switching of the ferroelectric domain in (100)-oriented PMN-0.3PT single crystal. The tri-layer multiferroic heterostructure showed a very large CME constant of 7.7 x 10^{-5} s/m related to the strain effect. Also, the damping constant increases by the application of the bipolar E field. Due to the strain effect from PMN-PT substrate under the application of E field, the tri-layer system undergoes a change of the interfacial properties. The static and dynamics results

confirm that the Pt layer undergoes a paramagnetic transition under the application of E field which led to the uncoupling between the upper and lower magnetic films.

Bibliography

[1] Claude Chappert, Albert Fert, and Frédéric Nguyen Van Dau. The emergence of spin electronics in data storage. *Nanoscience And Technology: A Collection of Reviews from Nature Journals*, pages 147–157, 2010.

[2] Andrew D Kent and Daniel C Worledge. A new spin on magnetic memories. *Nature nanotechnology*, 10(3):187–191, 2015.

[3] Yao Wang, Jiamian Hu, Yuanhua Lin, and Ce-Wen Nan. Multiferroic magnetoelectric composite nanostructures. *NPG Asia Materials*, 2(2):61–68, 2010.

[4] Ming Liu, Ziyao Zhou, Tianxiang Nan, Brandon M Howe, Gail J Brown, and Nian X Sun. Voltage tuning of ferromagnetic resonance with bistable magnetization switching in energy-efficient magnetoelectric composites. *Advanced Materials*, 25(10):1435–1439, 2013.

[5] Jia-Mian Hu, Zheng Li, Long-Qing Chen, and Ce-Wen Nan. High-density magnetoresistive random access memory operating at ultralow voltage at room temperature. *Nature communications*, 2(1):1–8, 2011.

[6] Manuel Bibes and Agnès Barthélémy. Towards a magnetoelectric memory. *Nature materials*, 7(6):425–426, 2008.

[7] Evgeny Y Tsymbal. Electric toggling of magnets. *Nature materials*, 11(1):12–13, 2012.

[8] Jia-Mian Hu, Long-Qing Chen, and Ce-Wen Nan. Multiferroic heterostructures integrating ferroelectric and magnetic materials. *Advanced materials*, 28(1):15–39, 2016.

[9] R Ramesh. N. and prospects in thin films," nature m a. *Spaldin,"Multiferroics: Progress aterials*, 6:21–29, 2007.

[10] Haribabu Palneedi, Venkateswarlu Annapureddy, Shashank Priya, and Jungho Ryu. Status and perspectives of multiferroic magnetoelectric composite materials and applications. In *Actuators*, volume 5, page 9. Multidisciplinary Digital Publishing Institute, 2016.

[11] W Jahjah, J-Ph Jay, Y Le Grand, A Fessant, J Richy, Cécile Marcelot, Bénédicte Warot-Fonrose, ARE Prinsloo, CJ Sheppard, DT Dekadjevi, et al. Influence of mesoporous or parasitic bifeo 3 structural state on the magnetization reversal in multiferroic bifeo 3/ni 81 fe 19 polycrystalline bilayers. *Journal of Applied Physics*, 124(23):235309, 2018.

[12] Junyi Zhai, Zengping Xing, Shuxiang Dong, Jiefang Li, and Dwight Viehland. Magnetoelectric laminate composites: an overview. *Journal of the American Ceramic Society*, 91(2):351–358, 2008.

[13] Nicola A Spaldin and Manfred Fiebig. The renaissance of magnetoelectric multiferroics. *Science*, 309(5733):391–392, 2005.

[14] W Eerenstein, M Wiora, JL Prieto, JF Scott, and ND Mathur. Giant sharp and persistent converse magnetoelectric effects in multiferroic epitaxial heterostructures. *Nature materials*, 6(5):348–351, 2007.

[15] Pengdi Han, Weiling Yan, Jian Tian, Xinling Huang, and Huixin Pan. Cut directions for the optimization of piezoelectric coefficients of lead magnesium niobate–lead titanate ferroelectric crystals. *Applied Physics Letters*, 86(5):052902, 2005.

[16] J Lou, David Reed, C Pettiford, M Liu, Pengdi Han, Shuxiang Dong, and NX Sun. Giant microwave tunability in fegab/lead magnesium niobate-lead titanate multiferroic composites. *Applied Physics Letters*, 92(26):262502, 2008.

[17] C Thiele, K Dörr, O Bilani, J Rödel, and L Schultz. Influence of strain on the magnetization and magnetoelectric effect in la 0.7 a 0.3 mn o 3/ pmn- pt (001)(a= sr, ca). *Physical Review B*, 75(5):054408, 2007.

[18] Tao Wu, Alexandre Bur, Ping Zhao, Kotekar P Mohanchandra, Kin Wong, Kang L Wang, Christopher S Lynch, and Gregory P Carman. Giant electric-field-induced reversible and permanent magnetization reorientation on magnetoelectric ni/(011)[pb (mg 1/3 nb 2/3) o 3](1- x)–[pbtio 3] x heterostructure. *Applied Physics Letters*, 98(1):012504, 2011.

[19] Ziyao Zhou, Brandon M Howe, Ming Liu, Tianxiang Nan, Xing Chen, Krishnamurthy Mahalingam, Nian X Sun, and Gail J Brown. Interfacial charge-mediated non-volatile magnetoelectric coupling in co 0.3 fe 0.7/ba 0.6 sr 0.4 tio 3/nb: Srtio 3 multiferroic heterostructures. *Scientific Reports*, 5(1):1–7, 2015.

[20] Carlos AF Vaz, Jason Hoffman, Charles H Ahn, and Ramamoorthy Ramesh. Magnetoelectric coupling effects in multiferroic complex oxide composite structures. *Advanced materials*, 22(26-27):2900–2918, 2010.

[21] Binod Paudel, Igor Vasiliev, Mahmoud Hammouri, Dmitry Karpov, Aiping Chen, Valeria Lauter, and Edwin Fohtung. Strain vs. charge mediated magnetoelectric coupling across the magnetic oxide/ferroelectric interfaces. *RSC advances*, 9(23):13033–13041, 2019.

[22] ZG Sun, H Kuramochi, M Mizuguchi, F Takano, Y Semba, and H Akinaga. Magnetic properties and domain structures of fesib thin films. *Surface science*, 556(1):33–38, 2004.

[23] Chikako Yokota, Kazushi Ishiyama, and Ken Ichi Arai. Comparison with film substrates of polyimide and ni for cantilevered magnetic actuators. *IEEJ Transactions on Electrical and Electronic Engineering*, 2(4):436–439, 2007.

[24] KI Arai, CS Muranaka, and M Yamaguchi. A new hybrid device using magnetostrictive amorphous films and piezoelectric substrates. *IEEE transactions on magnetics*, 30(2):916–918, 1994.

[25] Jaewon Shin, Sung Hoon Kim, Yasuaki Suwa, Shuichiro Hashi, and Kazushi Ishiyama. Control of in-plane uniaxial anisotropy of fe72si14b14 magnetostrictive thin film using a thermal expansion coefficient. *Journal of Applied Physics*, 111(7):07E511, 2012.

[26] SK Ghatak and A Mitra. Stress dependent magnetic properties of as-received and heat-pulse annealed amorphous fe81b13. 5si3. 5c2. *Solid state communications*, 68(11):997–1001, 1988.

[27] BD Cullity. Introduction to magnetic materials. addisonwesley series in metallurgy and materials, 1972.

[28] Nicola A Spaldin. *Magnetic materials: fundamentals and applications*. Cambridge university press, 2010.

[29] CH Ahn, KM Rabe, and J-M Triscone. Ferroelectricity at the nanoscale: local polarization in oxide thin films and heterostructures. *Science*, 303(5657):488–491, 2004.

[30] Li Jin, Fei Li, and Shujun Zhang. Decoding the fingerprint of ferroelectric loops: comprehension of the material properties and structures. In *Progress in Advanced Dielectrics*, pages 21–104. World Scientific, 2020.

[31] AA Bokov and Z-G Ye. Recent progress in relaxor ferroelectrics with perovskite structure. *Journal of materials science*, 41(1):31–52, 2006.

[32] Alexei A Bokov and Zuo-Guang Ye. Dielectric relaxation in relaxor ferroelectrics. *Journal of Advanced dielectrics*, 2(02):1241010, 2012.

[33] C Lei, Alexei A Bokov, and Z-G Ye. Ferroelectric to relaxor crossover and dielectric phase diagram in the ba ti o 3–ba sn o 3 system. *Journal of applied physics*, 101(8):084105, 2007.

[34] Alexei A Bokov, Brian J Rodriguez, Xiaohui Zhao, Jae-Hyeon Ko, Stephen Jesse, Xifa Long, Weiguo Qu, Tae Hyun Kim, John D Budai, Anna N Morozovska, et al. Compositional disorder, polar nanoregions and dipole dynamics in pb (mg1/3nb2/3) o3-based relaxor ferroelectrics. 2011.

[35] Huaxiang Fu and Ronald E Cohen. Polarization rotation mechanism for ultrahigh electromechanical response in single-crystal piezoelectrics. *Nature*, 403(6767):281–283, 2000.

[36] Manfred Fiebig. Revival of the magnetoelectric effect. *Journal of physics D: applied physics*, 38(8):R123, 2005.

[37] Ce-Wen Nan, MI Bichurin, Shuxiang Dong, D Viehland, and G Srinivasan. Multiferroic magnetoelectric composites: Historical perspective, status, and future directions. *Journal of applied physics*, 103(3):1, 2008.

[38] Jing Ma, Jiamian Hu, Zheng Li, and Ce-Wen Nan. Recent progress in multiferroic magnetoelectric composites: from bulk to thin films. *Advanced materials*, 23(9):1062–1087, 2011.

[39] Ramaroorthy Ramesh and Nicola A Spaldin. Multiferroics: progress and prospects in thin films. *Nature materials*, 6(1):21–29, 2007.

[40] Carlos AF Vaz. Electric field control of magnetism in multiferroic heterostructures. *Journal of Physics: Condensed Matter*, 24(33):333201, 2012.

[41] Nian X Sun and Gopalan Srinivasan. Voltage control of magnetism in multiferroic heterostructures and devices. In *Spin*, volume 2, page 1240004. World Scientific, 2012.

[42] LW Martin, SP Crane, YH Chu, MB Holcomb, M Gajek, Mark Huijben, Chan-Ho Yang, N Balke, and R Ramesh. Multiferroics and magnetoelectrics: thin films and nanostructures. *Journal of Physics: Condensed Matter*, 20(43):434220, 2008.

[43] Shuxiang Dong, Jinrong Cheng, JF Li, and D Viehland. Enhanced magnetoelectric effects in laminate composites of terfenol-d/pb (zr, ti) o 3 under resonant drive. *Applied Physics Letters*, 83(23):4812–4814, 2003.

[44] Ming Liu, Jing Lou, Shandong Li, and Nian X Sun. E-field control of exchange bias and deterministic magnetization switching in afm/fm/fe multiferroic heterostructures. *Advanced Functional Materials*, 21(13):2593–2598, 2011.

[45] Junyi Y Zhai, Shuxiang Dong, Zengping P Xing, Junqi Gao, Jiefang F Li, and D Viehland. Tunable magnetoelectric resonance devices. *Journal of Physics D: Applied Physics*, 42(12):122001, 2009.

[46] Hans Schmid. Multi-ferroic magnetoelectrics. *Ferroelectrics*, 162(1):317–338, 1994.

[47] Daniel Khomskii. Trend: Classifying multiferroics: Mechanisms and effects. *Physics*, 2:20, 2009.

[48] Chengliang Lu, Menghao Wu, Lin Lin, and Jun-Ming Liu. Single-phase multiferroics: new materials, phenomena, and physics. *National Science Review*, 6(4):653–668, 2019.

[49] JBNJ Wang, JB Neaton, H Zheng, V Nagarajan, SB Ogale, B Liu, D Viehland, V Vaithyanathan, DG Schlom, UV Waghmare, et al. Epitaxial bifeo3 multiferroic thin film heterostructures. *science*, 299(5613):1719–1722, 2003.

[50] T Kimura, T Goto, H Shintani, K Ishizaka, T-h Arima, and Y Tokura. Magnetic control of ferroelectric polarization. *nature*, 426(6962):55–58, 2003.

[51] N Hur, S Park, PA Sharma, JS Ahn, S Guha, and Sang-Wook Cheong. Electric polarization reversal and memory in a multiferroic material induced by magnetic fields. *Nature*, 429(6990):392–395, 2004.

[52] J Van Suchtelen. Product properties: a new application of composite materials. *Phillips Research Reports*, 27:28–37, 1972.

[53] RE Newnham, DP Skinner, and LE Cross. Connectivity and piezoelectric-pyroelectric composites. *Materials Research Bulletin*, 13(5):525–536, 1978.

[54] Sergey Lopatin, Irina Lopatina, and Inna Lisnevskaya. Magnetoelectric pzt/ferrite composite material. *Ferroelectrics*, 162(1):63–68, 1994.

[55] Andre K Geim and Konstantin S Novoselov. Nanoscience and technology: a collection of reviews from nature journals. *Assembly Autom*, 20:11–19, 2010.

[56] KY Choi, P Lemmens, G Güntherodt, M Pattabiraman, G Rangarajan, VP Gnezdilov, G Balakrishnan, D McK Paul, and MR Lees. Raman scattering study of nd1- xsrxmno3 (x= 0.3, 0.5). *Journal of Physics: Condensed Matter*, 15(19):3333, 2003.

[57] S Fusil, Vincent Garcia, A Barthélémy, and M Bibes. Magnetoelectric devices for spintronics. *Annual Review of Materials Research*, 44:91–116, 2014.

[58] Cheng Song, Bin Cui, Fan Li, Xiangjun Zhou, and Feng Pan. Recent progress in voltage control of magnetism: Materials, mechanisms, and performance. *Progress in Materials Science*, 87:33–82, 2017.

[59] B Cui, C Song, GY Wang, HJ Mao, F Zeng, and F Pan. Strain engineering induced interfacial self-assembly and intrinsic exchange bias in a manganite perovskite film. *Scientific reports*, 3(1):1–6, 2013.

[60] B Cui, C Song, F Li, GY Wang, HJ Mao, JJ Peng, F Zeng, and F Pan. Tuning the entanglement between orbital reconstruction and charge transfer at a film surface. *Scientific reports*, 4(1):1–8, 2014.

[61] B Cui, C Song, Y Sun, YY Wang, YL Zhao, F Li, GY Wang, F Zeng, and F Pan. Exchange bias field induced symmetry-breaking of magnetization rotation in two-dimension. *Applied Physics Letters*, 105(15):152402, 2014.

[62] Alexander J Grutter, Brian J Kirby, MT Gray, CL Flint, US Alaan, Y Suzuki, and Julie A Borchers. Electric field control of interfacial ferromagnetism in camno 3/caruo 3 heterostructures. *Physical review letters*, 115(4):047601, 2015.

[63] Martin Weisheit, Sebastian Fähler, Alain Marty, Yves Souche, Christiane Poinsignon, and Dominique Givord. Electric field-induced modification of magnetism in thin-film ferromagnets. *Science*, 315(5810):349–351, 2007.

[64] K Shimamura, D Chiba, S Ono, S Fukami, N Ishiwata, M Kawaguchi, K Kobayashi, and T Ono. Electrical control of curie temperature in cobalt using an ionic liquid film. *Applied Physics Letters*, 100(12):122402, 2012.

[65] Ying-Hao Chu, Lane W Martin, Mikel B Holcomb, Martin Gajek, Shu-Jen Han, Qing He, Nina Balke, Chan-Ho Yang, Donkoun Lee, Wei Hu, et al. Electric-field control of local ferromagnetism using a magnetoelectric multiferroic. *Nature materials*, 7(6):478–482, 2008.

[66] SM Wu, Shane A Cybart, P Yu, MD Rossell, JX Zhang, R Ramesh, and RC Dynes. Reversible electric control of exchange bias in a multiferroic field-effect device. *Nature materials*, 9(9):756–761, 2010.

[67] T Zhao, A Scholl, F Zavaliche, K Lee, M Barry, A Doran, MP Cruz, YH Chu, C Ederer, NA Spaldin, et al. Electrical control of antiferromagnetic domains in

multiferroic bifeo 3 films at room temperature. *Nature materials*, 5(10):823–829, 2006.

[68] Peter J Kelly and R Derek Arnell. Magnetron sputtering: a review of recent developments and applications. *Vacuum*, 56(3):159–172, 2000.

[69] Bertram Eugene Warren. *X-ray Diffraction*. Courier Corporation, 1990.

[70] D Lewis and DO Northwood. X-ray diffraction measurement of microstrains. *Strain*, 4(3):19–23, 1968.

[71] Joseph D Andrade. X-ray photoelectron spectroscopy (xps). In *Surface and interfacial aspects of biomedical polymers*, pages 105–195. Springer, 1985.

[72] Efrat Korin, Natalya Froumin, and Smadar Cohen. Surface analysis of nanocomplexes by x-ray photoelectron spectroscopy (xps). *ACS Biomaterials Science & Engineering*, 3(6):882–889, 2017.

[73] Daniel Rugar and Paul Hansma. Atomic force microscopy. *Physics today*, 43(10):23–30, 1990.

[74] Ricardo Garcıa and Ruben Perez. Dynamic atomic force microscopy methods. *Surface science reports*, 47(6-8):197–301, 2002.

[75] Simon Foner. Vibrating sample magnetometer. *Review of Scientific Instruments*, 27(7):548–548, 1956.

[76] Sadhan Chandra Das, Aga Shahee, NP Lalla, and T Shripathi. A simple and low cost sawyer-tower ferro-electric loop tracer with variable frequency and compensation circuit. In *Proceedings of the 54th DAE Solid State Physics Symposium Volume*, volume 54, pages 439–440, 2009.

[77] Xinger Zhao, Zhongqiang Hu, Qu Yang, Bin Peng, Ziyao Zhou, and Ming Liu.

Voltage control of ferromagnetic resonance and spin waves. *Chinese Physics B*, 27(9):097505, 2018.

[78] Tetsuya Osaka, Madoka Takai, Katsuyoshi Hayashi, Keishi Ohashi, Mikiko Saito, and Kazuhiko Yamada. A soft magnetic conife film with high saturation magnetic flux density and low coercivity. *Nature*, 392(6678):796–798, 1998.

[79] SN Piramanayagama. Applied physics reviews—focused review. *JOURNAL OF APPLIED PHYSICS*, 102:011301, 2007.

[80] Zhiguang Wang, Xinjun Wang, Menghui Li, Yuan Gao, Zhongqiang Hu, Tianxiang Nan, Xianfeng Liang, Huaihao Chen, Jia Yang, Syd Cash, et al. Highly sensitive flexible magnetic sensor based on anisotropic magnetoresistance effect. *Advanced Materials*, 28(42):9370–9377, 2016.

[81] Denny D Tang and Yuan-Jen Lee. *Magnetic memory: fundamentals and technology*. Cambridge University Press, 2010.

[82] John H van Vleck. On the anisotropy of cubic ferromagnetic crystals. *Physical Review*, 52(11):1178, 1937.

[83] Fanglin Che. *Methane steam reforming over Ni-based catalysts: Using electric fields to enhance catalytic performance*. Washington State University, 2016.

[84] Yi Qi and Michael C McAlpine. Nanotechnology-enabled flexible and biocompatible energy harvesting. *Energy & Environmental Science*, 3(9):1275–1285, 2010.

[85] M Gueye, BM Wague, F Zighem, M Belmeguenai, MS Gabor, T Petrisor Jr, C Tiusan, S Mercone, and D Faurie. Bending strain-tunable magnetic anisotropy in co2feal heusler thin film on kapton®. *Applied Physics Letters*, 105(6):062409, 2014.

[86] Xinyu Qiao, Baomin Wang, Zhenhua Tang, Yuan Shen, Huali Yang, Junling Wang, Qingfeng Zhan, Sining Mao, Xiaohong Xu, and Run-Wei Li. Tuning

magnetic anisotropy of amorphous cofeb film by depositing on convex flexible substrates. *AIP Advances*, 6(5):056106, 2016.

[87] Yungeun Ha, Ju-Hwan Baeg, Sungkyun Park, and Young-Rae Cho. Effect of substrate roughness and film thickness on the magnetic properties of cofeb films on polymer substrate. *Vacuum*, page 110399, 2021.

[88] Jodi M Iwata-Harms, Guenole Jan, Huanlong Liu, Santiago Serrano-Guisan, Jian Zhu, Luc Thomas, Ru-Ying Tong, Vignesh Sundar, and Po-Kang Wang. High-temperature thermal stability driven by magnetization dilution in cofeb free layers for spin-transfer-torque magnetic random access memory. *Scientific reports*, 8(1):1–7, 2018.

[89] Shuichiro Hashi, Daisuke Sora, and Kazushi Ishiyama. Strain and vibration sensor based on inverse magnetostriction of amorphous magnetostrictive films. *IEEE Magnetics Letters*, 10:1–4, 2019.

[90] Marco Coïsson, Franco Vinai, Paola Tiberto, and Federica Celegato. Magnetic properties of fesib thin films displaying stripe domains. *Journal of magnetism and magnetic materials*, 321(7):806–809, 2009.

[91] Hideo Ohno. A window on the future of spintronics. *Nature materials*, 9(12):952–954, 2010.

[92] Wilma Eerenstein, ND Mathur, and James F Scott. Multiferroic and magnetoelectric materials. *nature*, 442(7104):759–765, 2006.

[93] Ramaroorthy Ramesh and Nicola A Spaldin. Multiferroics: progress and prospects in thin films. *Nanoscience And Technology: A Collection of Reviews from Nature Journals*, pages 20–28, 2010.

[94] Eiji Saitoh. New order for magnetism. *Nature*, 455(7212):474–475, 2008.

[95] Jia-Mian Hu, Jing Ma, Jing Wang, Zheng Li, Yuan-Hua Lin, and CW Nan. Magnetoelectric responses in multiferroic composite thin films. *Journal of Advanced Dielectrics*, 1(01):1–16, 2011.

[96] Pavel Borisov, Andreas Hochstrat, Xi Chen, Wolfgang Kleemann, and Christian Binek. Magnetoelectric switching of exchange bias. *Physical review letters*, 94(11):117203, 2005.

[97] JT Heron, M Trassin, K Ashraf, M Gajek, Q He, SY Yang, DE Nikonov, YH Chu, S Salahuddin, and R Ramesh. Electric-field-induced magnetization reversal in a ferromagnet-multiferroic heterostructure. *Physical review letters*, 107(21):217202, 2011.

[98] James M Rondinelli, Massimiliano Stengel, and Nicola A Spaldin. Carrier-mediated magnetoelectricity in complex oxide heterostructures. *Nature nanotechnology*, 3(1):46–50, 2008.

[99] HL Meyerheim, F Klimenta, A Ernst, K Mohseni, S Ostanin, M Fechner, S Parihar, IV Maznichenko, I Mertig, and J Kirschner. Structural secrets of multiferroic interfaces. *Physical Review Letters*, 106(8):087203, 2011.

[100] J-M Hu, L Shu, Z Li, Y Gao, Y Shen, YH Lin, LQ Chen, and CW Nan. Film size-dependent voltage-modulated magnetism in multiferroic heterostructures. *Philosophical Transactions of the Royal Society A: Mathematical, Physical and Engineering Sciences*, 372(2009):20120444, 2014.

[101] Vladimir Koval, Giuseppe Viola, and Yongqiang Tan. Biasing effects in ferroic materials. *Ferroelectric Materials–Synthesis and Characterization*, 2015.

[102] Dragan Damjanovic. Hysteresis in piezoelectric and ferroelectric materials. Technical report, Academic Press, 2006.

[103] Seung-Eek Park and Thomas R Shrout. Ultrahigh strain and piezoelectric behavior in relaxor based ferroelectric single crystals. *Journal of applied physics*, 82(4):1804–1811, 1997.

[104] HH Wu and RE Cohen. Electric-field-induced phase transition and electrocaloric effect in pmn-pt. *Physical Review B*, 96(5):054116, 2017.

[105] Ryusuke Hasegawa. Design and fabrication of new soft magnetic materials. *Journal of non-crystalline solids*, 329(1-3):1–7, 2003.

[106] JR Childress, R Kergoat, O Durand, J-M George, P Galtier, J Miltat, and A Schuhl. Magnetic properties and domain structure of epitaxial (001) fe/pd superlattices. *Journal of magnetism and magnetic materials*, 130(1-3):13–22, 1994.

[107] O Durand, JR Childress, P Galtier, R Bisaro, and A Schuhl. Origin of the uniaxial magnetic anisotropy in fe films grown by molecular beam epitaxy. *Journal of magnetism and magnetic materials*, 145(1-2):111–117, 1995.

[108] Darrell G Schlom, Long-Qing Chen, Chang-Beom Eom, Karin M Rabe, Stephen K Streiffer, and Jean-Marc Triscone. Strain tuning of ferroelectric thin films. *Annu. Rev. Mater. Res.*, 37:589–626, 2007.

[109] Ming Zheng, Takamasa Usami, and Tomoyasu Taniyama. Shear-strain-mediated large nonvolatile tuning of ferromagnetic resonance by an electric field in multiferroic heterostructures. *NPG Asia Materials*, 13(1):1–9, 2021.

[110] Yaming Zhou, Qiang Li, Fangping Zhuo, Chao Xu, Qingfeng Yan, Yiling Zhang, and Xiangcheng Chu. Domain switching and polarization fatigue in rhombohedral pin-pmn-pt and mn-doped pin-pmn-pt single crystals. *Journal of the American Ceramic Society*, 102(11):6668–6679, 2019.

[111] Steffen Oswald. X-ray photoelectron spectroscopy in analysis of surfaces. *Encyclopedia of Analytical Chemistry: Applications, Theory and Instrumentation*, 2006.

[112] Weiwei Lin, Nicolas Vernier, Guillaume Agnus, Na Lei, Sylvain Eimer, and Dafiné Ravelosona. Interfacial charge accumulation effect on magnetic domain wall nucleation and propagation in a pt/co/pt/al2o3 structure. *arXiv preprint arXiv:1201.5917*, 2012.

[113] Michael Farle. Ferromagnetic resonance of ultrathin metallic layers. *Reports on progress in physics*, 61(7):755, 1998.

[114] Ming Liu, Ogheneyunume Obi, Jing Lou, Yajie Chen, Zhuhua Cai, Stephen Stoute, Mary Espanol, Magnum Lew, Xiaodan Situ, Kate S Ziemer, et al. Giant electric field tuning of magnetic properties in multiferroic ferrite/ferroelectric heterostructures. *Advanced Functional Materials*, 19(11):1826–1831, 2009.

[115] Aaron L Stancik and Eric B Brauns. A simple asymmetric lineshape for fitting infrared absorption spectra. *Vibrational Spectroscopy*, 47(1):66–69, 2008.

[116] Yang Cheng, Aidan J Lee, Jack T Brangham, Shane P White, William T Ruane, P Chris Hammel, and Fengyuan Yang. Thickness and angular dependent ferromagnetic resonance of ultra-low damping co25fe75 epitaxial films. *Applied Physics Letters*, 113(26):262403, 2018.

[117] LAURA GREENE, TOM Lubensky, MATTHEW TIRRELL, PAUL CHAIKIN, HONG DING, KATHERINE FABER, PAULA HAMMOND, CHRISTINE HECKLE, KEVIN HEMKER, JOSEPH HEREMANS, et al. Frontiers of materials research: A decadal survey. Technical report, The National Academies of Sciences, Engineering and Medicine, 2019.

[118] YT Yang, J Li, XL Peng, B Hong, XQ Wang, HL Ge, DH Wang, and YW Du.

Surface-effect enhanced magneto-electric coupling in fept/pmn-pt multiferroic heterostructures. *AIP Advances*, 7(5):055833, 2017.

[119] BY Zong, GC Han, YK Zheng, ZB Guo, KB Li, L Wang, JJ Qiu, ZY Liu, LH An, P Luo, et al. Ultrasoft and high magnetic moment nife film electrodeposited from a cu^{2+} contained solution. *IEEE transactions on magnetics*, 42(10):2775–2777, 2006.

[120] Bonkeup Koo and Bongyoung Yoo. Electrodeposition of low-stress nife thin films from a highly acidic electrolyte. *Surface and Coatings Technology*, 205(3):740–744, 2010.

[121] VB Naik, H Meng, JX Xiao, RS Liu, A Kumar, KY Zeng, P Luo, and S Yap. Effect of electric-field on the perpendicular magnetic anisotropy and strain properties in cofeb/mgo magnetic tunnel junctions. *Applied Physics Letters*, 105(5):052403, 2014.

[122] Wei Li, Yi Zeng, Zijing Zhao, Biao Zhang, Junjie Xu, Xiaoxiao Huang, and Yanglong Hou. 2d magnetic heterostructures and their interface modulated magnetism. *ACS Applied Materials & Interfaces*, 13(43):50591–50601, 2021.

[123] Kritsanu Tivakornsasithorn, Taehee Yoo, Hakjoon Lee, Sangyeop Lee, Seonghoon Choi, Seul-Ki Bac, Kyung Jae Lee, Sanghoon Lee, Xinyu Liu, M Dobrowolska, et al. Magnetization reversal and interlayer exchange coupling in ferromagnetic metal/semiconductor fe/gamnas hybrid bilayers. *Scientific reports*, 8(1):1–11, 2018.

[124] Tomohiro Taniguchi, Julie Grollier, and Mark D Stiles. Spin-transfer torques generated by the anomalous hall effect and anisotropic magnetoresistance. *Physical Review Applied*, 3(4):044001, 2015.

[125] Minoru Yafuso, Keishi Miyazaki, Yusei Takayama, Sora Obinata, and Takashi

Kimura. Nonlinear power dependence of ferromagnetic resonance in nife/pt/cofeb trilayer. *Journal of Physics: Condensed Matter*, 34(4):045801, 2021.

[126] Anatolii F Kravets, AN Timoshevskii, BZ Yanchitsky, Michael A Bergmann, Johannes Buhler, Sebastian Andersson, and Vladislav Korenivski. Temperature-controlled interlayer exchange coupling in strong/weak ferromagnetic multilayers: A thermomagnetic curie switch. *Physical Review B*, 86(21):214413, 2012.

[127] Xiaoyong Liu, Wenzhe Zhang, Matthew J Carter, and Gang Xiao. Ferromagnetic resonance and damping properties of cofeb thin films as free layers in mgo-based magnetic tunnel junctions. *Journal of Applied Physics*, 110(3):033910, 2011.

[128] S Azzawi, AT Hindmarch, and D Atkinson. Magnetic damping phenomena in ferromagnetic thin-films and multilayers. *Journal of Physics D: Applied Physics*, 50(47):473001, 2017.